www.elsevier.com/locate/pquantelec

Next-generation thermo-plasmonic technologies and plasmonic nanoparticles in optoelectronics

Luciano De Sio, Tiziana Placido, Roberto Comparelli, M. Lucia Curri, Marinella Striccoli, Nelson Tabiryan, Timothy J. Bunning

PII: S0079-6727(15)00017-8
DOI: http://dx.doi.org/10.1016/j.pquantelec.2015.03.001
Reference: JPQE186

To appear in: *Progress in Quantum Electronics*

Cite this article as: Luciano De Sio, Tiziana Placido, Roberto Comparelli, M. Lucia Curri, Marinella Striccoli, Nelson Tabiryan, Timothy J. Bunning, Next-generation thermo-plasmonic technologies and plasmonic nanoparticles in optoelectronics, *Progress in Quantum Electronics,* http://dx.doi.org/10.1016/j.pquantelec.2015.03.001

Next-generation thermo-plasmonic technologies and plasmonic nanoparticles in optoelectronics

Luciano De Sio[1,2*], Tiziana Placido[3,4], Roberto Comparelli[4], M. Lucia Curri[4], Marinella Striccoli[4], Nelson Tabiryan[1], Timothy J. Bunning[5]

[1]Beam Engineering for Advanced Measurements Company, Winter Park, Florida 32789, USA

[2]Department of Physics - University of Calabria Centre of Excellence for the Study of Innovative Functional Materials 87036 Arcavacata di Rende, Italy

[3]Università degli Studi di Bari – Dip. Chimica, Via Orabona 4, 70126 - Bari, Italy
[4]CNR-IPCF Istituto per i Processi Chimici e Fisici, Sez. Bari, c/o Dip. Chimica Via Orabona 4, 70126 - Bari, Italy

[5]Air Force Research Laboratory, Wright-Patterson Air Force Base, Ohio 45433-7707, USA

**Corresponding author:* luciano.desio@fis.unical.it

Abstract

Controlling light interactions with matter on the nanometer scale provides for compelling opportunities for modern technology and stretches our understanding and exploitation of applied physics, electronics, and fabrication science. The smallest size to which light can be confined using standard optical elements such as lenses and mirrors is limited by diffraction. Plasmonic nanostructures have the extraordinary capability to control light beyond the diffraction limit through an unique phenomenon called the localized plasmon resonance. This remarkable capability enables unique prospects for the design, fabrication and characterization of highly integrated photonic signal-processing systems, nanoresolution optical imaging techniques and nanoscale electronic circuits. This paper summarizes the basic principles and the main achievements in the practical utilization of plasmonic effects in nanoparticles. Specifically, the paper aims at highlighting the major contributions of nanoparticles to nanoscale temperature monitoring, modern "drug free" medicine and the application of nanomaterials to a new generation of opto-electronics integrated circuits.

Keywords: Plasmonics, Nanomaterials, Soft Matter, Nanomedicine, Optoelectronics.

Contents

1. Introduction

Plasmonics is a subfield of nanophotonics, utilizing surface plasmons to control light at the nanoscale by coherent coupling of photons to free electron oscillations at the interface between a conductor and a dielectric. This field of research has emerged as an extremely promising technology with several main fields of application including information technology, solar energy, high-density data storage, life sciences and security. One promising way to localize the optical radiation into a nanometer-sized volume has been realized by using the unique properties of plasmonic metallic nanoparticles which represent an effective bridge between bulk materials and atomic/molecular structures. Nanoparticles can exhibit highly vibrant colors which are absent both from bulk material and individual atoms. The physics behind this phenomenon is based on the collective oscillation of conducting free electrons of the metallic nanoparticles, an effect referred to as a localized plasmonic resonance. The frequency of the resonance can be controlled by varying both the size and the shape of the nanoparticles and the dielectric constant of the surrounding medium. The optical properties of nanoparticles are determined by a set of parameters that include composition, particle size and shape, geometry, and local environment. Theory predicts that plasmons on neighbouring nanoparticles interact, mix and hybridize in a manner similar to the electronic wave functions of simple atomic and molecular orbitals. Nanoparticles can be potential key components in miniaturized all-optical computing nanocircuits due to their capability of confining light at the nanoscale below the diffraction limit of light by exploiting localized plasmonic resonance. Nanoparticles can also have a large technological impact in sensing and energy-harvesting applications as well as in the medical domain as active elements in photothermal therapy. This paper reviews some recent efforts utilizing nanoparticles in a number of research fields that including physics, chemistry, photonics, optics, medicine and electronics. First, we describe the optical properties of nanoparticles including the general methods used for their synthesis and surface chemistry modification. Such nanoparticles can be thought of as plasmonic atoms which assemble into well-defined clusters with customizable optical properties. This organization of plasmonic nanoparticles in architectures ranges from small clusters, chains, and 2-3D assemblies comprising thousands of nanoparticles hierarchically assembled is briefly reviewed. Next, the physics of heat generation in nanoparticles is described when stimulated with the correct frequency of laser light. The experimental methods that have been developed in order to detect nanoscale temperature variations will be briefly explored. Finally, some recent applications of nanoparticles are discussed including photo-thermal cancer therapy and nanoscale electronic

circuitry. In this review, attention is focused mainly on gold (Au) and silver (Ag) nanoparticles, the most widely exploited elements for plasmonic nanostructures in the community.

2. Optical properties of metal nanoparticles

The properties of bulk materials typically depend mainly on the type of chemical bond, not the size and shape of the construct. Conversely, semiconductor, metal and oxide nanoclusters in the nanoscale regime show interesting size-dependent optical, electronic, and chemical properties. Nanoparticles or clusters are defined as particles composed of a limited number of atoms ranging from 3 to 10^7.[1] Nanoparticles within this size domain are intermediate between the atomic/molecular size regimes and the macroscopic bulk size regime. At the nanoscale, the theories of classical and quantum mechanics are no longer valid and a rich variety of unexpected properties are possible. Nanoscience and nanotechnology have revolutionized science and engineering development at an ever increasing rate, driven by the desire to fabricate materials with novel and improved properties that will impact all areas of physical and chemical sciences, biological sciences, health sciences. The interesting optical properties of metal nanoparticles, including their bright intense colors, are due to their unique interaction with light. The metals Cu, Ag and Au are all elements belonging to the 11th group of the periodic table. The electron configurations of these elements are exceptions to the Madelung rule which describes the filling order of the atomic subshells. All of these elements have completely filled *d*-subshells (respectively 3d, 4d and 5d) and thus their core electrons reside in an inert gas configuration. Their metallic properties result from the lone valence electron in the half-filled *s*-subshells (4s, 5s and 6s respectively). The band structure of gold displays five comparatively flat *d*-bands, lying 1–3 eV below the Fermi energy, in which the ten *d*-electrons are located. The lone *s*-electron forms an *sp*-hybridized bond which is filled up to the Fermi energy. Electrons in this band can oscillate quasi-free due to the near parabolic shape of the band. This band structure defines the characteristic properties of these metals including their thermal and electrical conductivity. In the presence of an oscillating electromagnetic field, the conduction band free electrons of the metal undergo collective oscillations in resonance with the frequency of light. This process is resonant at a particular frequency of the light and is known as the plasmon resonance. Depending on the boundary conditions, it is commonly accepted to distinguish bulk plasmons, surface propagating plasmons or surface plasmon polaritons (2D films), and surface localized plasmons (nanoparticles). In particular, the surface plasmon polaritons propagate along metal surfaces in a waveguide-like fashion. In our case, we consider only nanoparticle based localized plasmons where the electric component of an external optical field

exerts a force on the conductive electrons and displaces them from their equilibrium positions to create uncompensated charges at the nanoparticle surface (Figure 1). These oscillations are called ‘‘localized surface’’ plasmons, have a well-defined resonance frequency, and arise due to polarization of the particle surface. The electronic oscillation can be simply illustrated as a photon confined to the small size of the nanostructure thus establishing an intense electric field around the particle. A net charge difference exists at the nanoparticle surface which, in turn, acts as a restoring force. In the simplest case, a dipolar oscillation of all the electrons with the same phase is created.[2,3] The surface plasmon oscillation decays by radiating its energy resulting in light scattering or nonradiatively converting absorbed light to heat.[4] Noble metals such as Cu, Ag, and Au have a strong plasmon resonance in the visible part of the spectrum whereas most other transition metals show only a broad and poorly resolved absorption band in the ultraviolet region. This difference is attributed to the strong coupling between the plasmon transition and the interband excitation. This gives electrons in the noble metals a high polarizability, which shifts the plasmon resonance to lower frequencies with a sharp bandwidth. The characteristic color of colloidal solutions of noble metal nanoparticles originates from this strong absorption when the frequency of the electromagnetic field becomes resonant with the coherent electron motion. Since copper is easily oxidized, Au and Ag nanostructures have been the most attractive for optical and sensing applications. The position, shape and intensity of the plasmon resonance strongly depends on various factors, including the dielectric constant of the surrounding medium, the electronic interactions between the stabilising ligands and the nanoparticle (which alter the electron density inside the nanoparticle), and the size, shape and monodispersity of the nanoparticles. Theoretical descriptions of the plasmon resonance and the main factors impacting its position, intensity and breadth have been prevalent in the literature recently. The interesting work of Kreibig and Vollmer gives a broad overview of the main existing plasmon band theories [2] whereas a comprehensive review focusing on Mie and effective medium theory has been published by Liz-Marzan[5]. Kelly and co-workers proposed methods to solve Maxwell equations in order to describe the optical properties of nanoparticles with arbitrary shape [6]. Other papers explain the fundamental relationships, including the size dependence of the plasmon bandwidth [7] or localized plasmon bands [8]. In the present work, we review the physics behind the phenomenon using two traditional theories including the Drude–Maxwell model and the theory proposed by Mie correlating the position, intensity and shape of the plasmon resonance with different parameters. As a first approach, the interaction of light with a small particle can be described by classical electrodynamics (Figure 1). This description relies on the knowledge of material parameters, including the complex

dielectric function ε(ω). Even when the dielectric function is known, the electrodynamical models assume idealized geometries, i.e. perfectly sharp interfaces. Even with these limations, many important features observed experimentally for particle plasmons can be understood using these simple considerations. The general solution of the interaction problem of a single homogeneous sphere of the radius R and of arbitrary material with an incident electromagnetic field was first given by G. Mie in 1908.[9] Mie presented a solution to Maxwell's equations that describes the extinction spectra of spherical particles of arbitrary size embedded in a homogeneous medium. The power of this method was splitting of the problem into two independent parts, including the solution of Maxwell's equations, and the determination of the dielectric constant. In his calculation, Mie introduces the dielectric function ε(ω, R) at the angular frequency ω in order to study the correlation between the frequency of the plasmon resonance and the dielectric function of the surrounding medium.

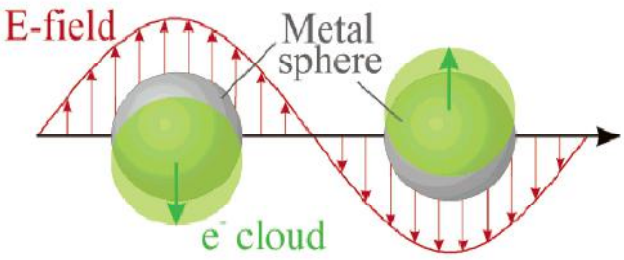

Figure 1: Schematic representation of the interaction of a small metal nanoparticle with light (not to scale, it represents a particle much smaller than the light wavelength) For simplicity only the electric field is represented. Reprinted with permission from ref. [6]

The spherical symmetry suggested the use of multipole (dipole, quadrupole, etc.) extensions of the fields, for the absorption and the scattering cross section of the particles as a function of the particle radius. The extinction spectrum then consists of both absorption and scattering modes, each of which has a contribution that depends on the particle size. Higher-order modes become more dominant with increasing particle size. Physically, this can be explained by the fact that for larger particles, light cannot polarize the nanoparticles homogeneously and retardation effects lead to the excitation of higher-order modes. Although Mie's theory describes accurately the optical extinction spectra of metal nanoparticles, it does not explain the physical process of the collective oscillation of the conduction band electrons. For nanoparticles which are much smaller than the wavelength of the interacting light, only the dipole oscillation contributes significantly to the extinction cross-section which can be calculated using the quasistatic approximation, introduced first by Rayleigh

who studied the scattering of light from small particles.[10] With this approximation, the electric field inside the particle is uniform and induces a dipole oscillation moment defined as:

$$\vec{p}(t) = \varepsilon_0 \varepsilon_m \alpha \vec{E}(t) \quad (1)$$

where ε_0 is the vacuum dielectric constant, α is the polarizability of the particle, and ε_m is the dielectric constant of the medium. The polarizability is obtained from the frequency-dependent dielectric constants of particle. For a sphere of volume V , the polarizability is given by the Clausius-Mossotti expression:

$$\alpha = 3V \frac{\varepsilon - \varepsilon_m}{\varepsilon + 2\varepsilon_m} \quad (2)$$

where $\varepsilon = \varepsilon_1 + i\varepsilon_2$ is the complex dielectric function of the sphere. The scattering and absorption cross sections are:

$$\sigma_{sca}(\omega) = \frac{8\pi^3 \omega^4}{3c^4} |\alpha(\omega)|^2 \quad (3)$$

$$\sigma_{abs}(\omega) = \frac{2\pi\omega}{c} Im\{\alpha(\omega)\} \quad (4)$$

and

$$\sigma_{ext}(\omega) = \sigma_{abs}(\omega) + \sigma_{sca}(\omega) \quad (5)$$

where c is the speed of light and ω is the angular frequency. The absorption of light is proportional linearly to the polarizability and thus to the volume of the particles, while the scattering scales with the square of the volume. Scattering therefore dominates the extinction of light for large particles, while absorption dominates for small particles. For particles smaller than 40 nm, scattering can be neglected and the particle is in a resonance condition when:

$$\varepsilon_1 = -2\varepsilon_m \quad (6)$$

If ω_p is defined as the resonance frequency that fulfils this condition, in the case of a free sphere, i.e. $\varepsilon_m = 1$, the absorption cross section can be expressed as:

$$(\omega, \omega_p) = \frac{V\omega}{c} \frac{[\varepsilon_1(\omega_p) - 1]^2 \varepsilon_2(\omega)}{[\varepsilon_1(\omega) - \varepsilon_1(\omega_p)]^2 + [\varepsilon_2(\omega)]^2} \quad (7)$$

The real and imaginary parts of the dielectric function describe the polarization of matter and the energy dissipated under interaction with an electromagnetic field, respectively. An accurate description is given by the Drude-Sommerfield theory [11,12] which depicts the electrons as a gas of independent, quasi-free point-shaped particles that are accelerated by an external electric field and slow down after a mean free time, $\tau = \Gamma^{-1}$ (for gold: τ = 30 fs at 273 K). This model determines the dielectric function, $\varepsilon(\omega)$ of a macroscopic metal by calculating the behavior of a single conduction electron and multiplying this behavior by the number of electrons present. This is only valid when assuming the independence of the single electrons, and leads to the dielectric function of a system of n free electrons per unit volume:

$$\varepsilon(\omega) = 1 - \frac{\omega_p^2}{\omega^2 + i\Gamma\omega} \tag{8}$$

determined by the plasma frequency $\omega_p = \sqrt{ne^2/\varepsilon_0 m^*}$ and by the relaxation constant, Γ. The dielectric function, $\varepsilon(\omega)$, is commonly expressed in terms of the electric susceptibility, χ. The previous equation becomes:

$$\varepsilon(\omega) = 1 + \chi_{DS}(\omega) \tag{9}$$

where χ_{DS} is the free-electron Drude-Sommerfield susceptibility. Electrons in a real metallic lattice are only quasi-free due to the lattice periodicity. The coupling of the free electrons to the ion core is taken into consideration by replacing the electron mass, m_e, with an effective electron mass, m_*, effectively altering ω_p. Electrons from deeper levels can also contribute to the dielectric function leading to an additional term in the above equation:

$$\varepsilon(\omega) = 1 + \chi_{DS} + \chi_{IB} \tag{10}$$

where the interband susceptibility $\chi_{IB} = \chi_{IB1} + i\chi_{IB2}$. The imaginary part describes direct energy dissipation and is large only for frequencies at which interband transitions occur. The real part is also for smaller frequencies. In this approximation, the surface plasmon resonance is independent of the particle size. This contradicts experimental results on metal nanoparticles much smaller than 10 nm [13] where the plasmon band shows a size dependence for small particles and disappears completely for nanoparticles $\leq$ 2 nm. The assumption of a free electron gas is not valid in the size range below 2 nm. In the Drude free-electron model, the dielectric function is modified for the smaller sized nanoparticles, by its factorization into two contributions, the interband transitions and a free electron part. This second term can be modified to account for enhanced electron-surface

scattering as a function of particle size. The dielectric function becomes size dependent. Other effects including the "spill out" of the conduction electrons have been considered and incorporated into explaining the bulk dielectric function appropriately. Mie's theory and experimental spectra result in good agreement for nanoparticles larger than 20 nm, up to the bulk metals, that is when the normal incidence absorption does not shows any longer a plasmon resonance. The spectrum is composed of the sum of size-dependent absorption and scattering modes.

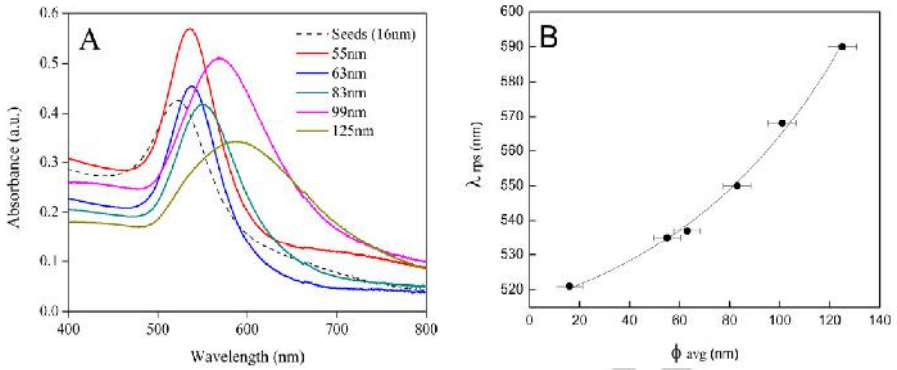

Figure 2: UV–visible absorption spectra and absorption shift of Au nanoparticles. (A) UV–visible absorption spectrum of the synthetized Au nanoparticles. (B) Shift in absorption of Au nanoparticles with particle size. Reprinted with permission from ref. [14]

Higher order modes become more dominant with increasing particle size, causing the plasmon absorption band to red shift and increase bandwidth as the light cannot polarize the nanoparticles homogeneously and retardation effects lead to the excitation of higher order modes.[2] In Figure 2 the absorption spectra of spherical Au nanoparticles with different sizes are shown. As the size increases, the plasmon band shifts to the red. In addition, the surface plasmon absorption maximum and bandwidth depend on the particle shape in addition to size. When the particle shape is not spherical, the surface geometry modulates the electric field intensity on the surface. This gives rise to a change in the oscillation frequency of the electrons, generating different cross-sections for the optical properties including absorption and scattering. The theoretical explanation of the localized plasmonic resonance dependence from particle shape has been explained by Gans, by extending Mie's theory to cylindrical and oblate metal nanoparticles.[15] Recent methods including the discrete dipole approximation (DDA) and finite difference time domain methods (FDTD) use numerical approaches to calculate the localized plasmonic resonance absorption for an arbitrary geometry.[1] Particles are usually characterized by their aspect ratio (length over width of the particle). In anisotropic particles, the localized plasmonic resonance absorption is shifted in the red region of the spectrum as the spacing between particles is reduced, and this shift is well described as an exponential function of the gap between the two particles. It

becomes negligible when the gap is larger than 2.5 times the short-axis length.[16] A red shift for a polarization parallel to the long particle axis and a blue shift for the orthogonal polarization have been reported and rationalized by dipolar interaction mechanisms.[17] Cylindrical shaped nanoparticles, or nanorods, exhibit two plasmon resonances [18], one due to the transverse oscillation of the electrons, positioned around 520 nm for Au, and the other due to the longitudinal plasmon resonance at longer wavelengths, as shown for various aspect ratios in Figure 3.

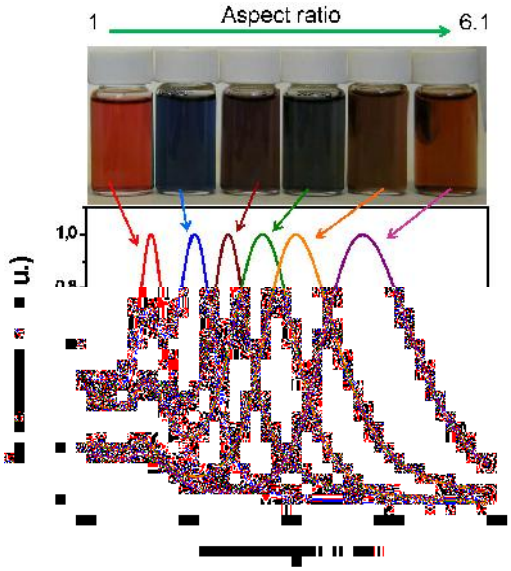

Figure 3: Shape dependence of surface plasmon resonance of Au nanorods with different aspect ratio.

The transverse localized plasmonic resonance does not depend on the aspect ratio and is at the same wavelength as that of spherical nanoparticles. The longitudinal localized plasmonic resonance increases with larger aspect ratios, allowing tuning across the visible region. Nanorods have attracted much recent attention [19–21] due to the ease of preparation, the large number of synthetic methods available, the high monodispersity possible, and the experimental control over the aspect ratio. The plasmon absorption of metal nanoparticles is also sensitive to the surrounding environment as changes in the dielectric constant of the surrounding material will affect the oscillation frequency. Medium effects can be classified into two general categories including solvents that alter the refractive index of the environment surrounding the nanoparticle and solvents that complex with the metal surface itself. The latter effect is most important as chemically bonded molecules induce facile changes of the electron density on the surface resulting in frequency shifts. [22]

3. Synthesis of metal nanoparticles

Common plasmonic materials include the noble metals, Au and Ag, but also include Cu, aluminum, highly doped oxides and chalcogenides, and graphene. Nanostructures based on these diverse materials show dramatically distinct plasmonic behavior due to differences in carrier concentration, carrier mobility, and Ohmic loss. In particular, Ag and Au are the most investigated materials, due to the enormous success in using chemical methods to finely control their growth.. These two elements also exhibit peak plasmon frequencies in the visible region of the spectrum. In this review attention is mainly focused on Au due to its high oxidative stability, an advantage over Ag nanoparticles. Different shapes lead to different optical properties as summarized in Figure 4. Architectural control can enhance the optical properties and can be achieved by the synthesis of spheres, rods, core-shell, nanoshell, dimers, and branched structures. Fabrication from suitable metal nanostructure precursor can occur by both chemical and physical interactions. Critical prerequisites are the production of high-quality metallic structures with tunable size and controllable shapes. The field of nanoplasmonics has greatly benefited from advances in synthetic nanoparticle strategies that have occurred over the last decade.

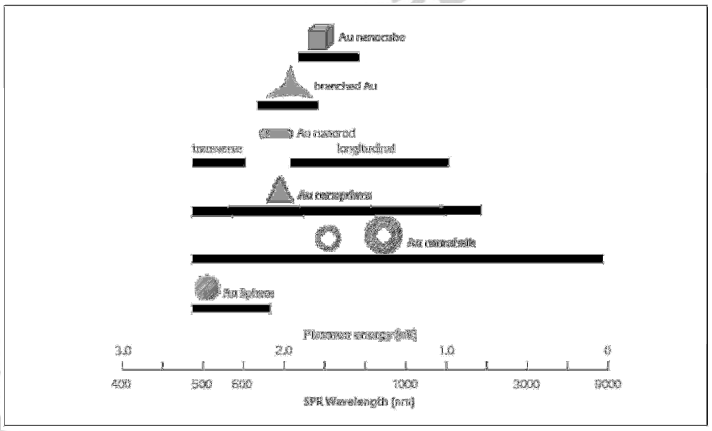

Figure 4: Range of plasmon resonance of Au nanoparticles as a function of their morphology. Reprinted with permission from ref. [23]

a. Physical methods

Some of the most innovative physical methods are based on the growth of metal nanostructures directly from the surface of suitable substrates.[23] These techniques are usually exploited to build devices for optoelectronic and plasmonic applications. *Laser ablation*, first introduced by Cotton et al. [24], represents one of the most popular preparative approaches and in recent years has emerged as an alternative to traditional chemical reduction methods for obtaining metal (Au, Ag, Pt)

nanoparticles in aqueous or in organic solvents without the use of any stabilizing molecule.[25] The general synthetic scheme involves the condensation of a plasma plume formed by the laser ablation of a bulk metal plate dipped in a liquid solution. As an example, Meunier's group developed a two-step femtosecond laser-assisted technique which produced size-controlled (2–80 nm) and functionalized spherical Au nanoparticles with a size distribution around 20%.[26] There are some limitations in the size and size distribution control of metal nanoparticles produced using this technique. *Electron-beam lithography* (EBL) is also widely used enabling multiple-shape nanostructures with size control on the tens of nanometer length scale. This technique has been used to pattern arrays of Au nanowires (of controllable length) linking two large electrodes on substrates coated with a film of SiO_2 (Figure 5a-c) [27] and to obtain "bowtie" nanoantennas on top of freestanding silicon nitride membranes (Figure 5d-f). This latter geometry can act as a nanoscale detector that converts local optical intensity variations into temperature variations [28]

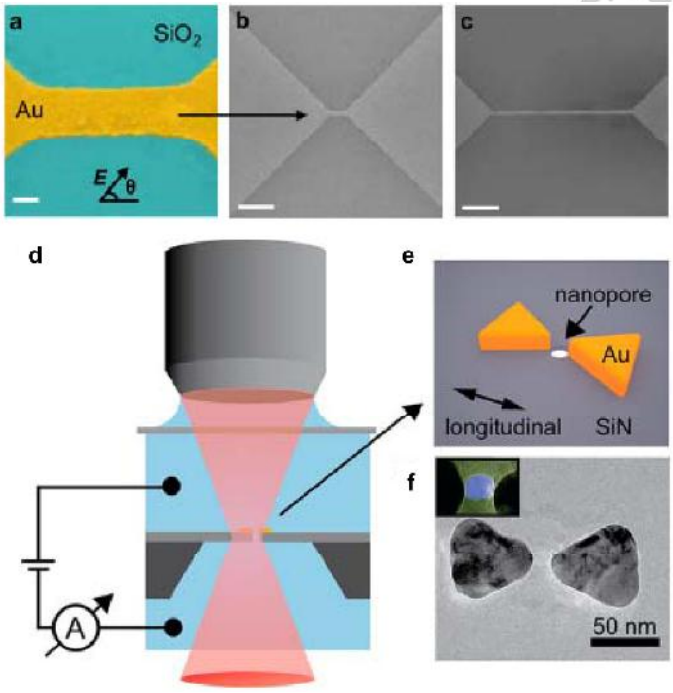

Figure 5: **(a–c)** Scanning electron microscope images of representative devices. **(a)** Au nanowire on 0.2 μm of SiO_2 with reference angle for polarization studies, **(b)** typical overall device geometry, **(c)** elongated design; **(d–f)** The principle of plasmonic nanopore optical profiling. **(d)** Schematic representation of the concept. Variations in the local optical intensity within a focal volume modulate the heating of nanoplasmonic structure. These temperature changes are measured electrically through changes in the ionic current through the nanopore. Optical intensity distributions are obtained by scanning the plasmonic nanopore in three dimensions using a piezoelectric stage. **(e)** 3D schematic representation of the plasmonic nanopore probe consisting of a plasmonic "bowtie" nanoantenna with a nanopore in the gap. **(f)** Transmission electron microscope image of a typical plasmonic nanopore. The inset shows a zoomed image of the 10 nm nanopore in the gap between the two Au triangles. Reprinted with permission from refs. [27, 28]

Another approach, *chemical vapour deposition,* has been used to deposit Au nanoparticles on ordered mesoporous molecular sieves by evaporation of an Au precursor heated to a fixed temperature. The precursor adsorbs on suitable substrates and undergoes calcination to decompose into metallic Au nanoparticles on the substrate surface.[29]

Pulsed laser deposition exploits a high-power pulsed laser beam focused inside a vacuum chamber to vaporize a target material which is then deposited as a thin film on a substrate (such as a silicon wafer facing the target). As an example, a highly dense and uniform layer of Au nanoparticles was produced on a poly(3,4-ethylenedioxythiophene):poly(styrene sulfonate) (PEDOT:PSS) film at room temperature as a means towards an improved efficiency photovoltaic device.[30] *Nanosphere lithography* [31] (also termed *colloidal lithography* [32]) is a powerful technique to inexpensively produce nanoparticle arrays with controlled shape, size and interparticle spacing. *The* self-assembly of monodisperse nanospheres and bulk spheres made, for instance, of polystyrene, will yield a two dimensional ordered crystal deposition mask on a Si substrates. Gold can then be deposited by thermal evaporation, electron beam deposition, or pulsed laser deposition. Mask removal leaves surface-confined nanoparticles on the substrate. Hexagonal arrays of nano-triangles or Au nano-ring arrays with different unit lattices have been fabricated from a double-layered mask.[31] Thermal annealing can also be used to transform the shape of the resulting nanoparticles from triangular Au plates to rounded Au nanoparticles.[33]

Ion Beam Sputtering is based on a defocused ion beam which destabilizes an otherwise flat surface, dislocating mobile adatoms and vacancies which re-arrange themselves *via* thermally activated diffusion, producing an array of periodic nano-structures (ripples, mounds, pyramids) which select a preferential periodicity (10nm – 500nm range). This technique shows promise as a fast method to sculpt surfaces at the nanometer scale and shows the ability to induce functional modification of the substrate.[34] As an example, Au nanowires have been prepared in vacuum conditions with the ion beam incident on polycrystalline metal surfaces (Au), resulting in a flat Au film exhibiting a dominant population of grains with a diameter peaked around 80 nm.[35] *Dip-pen nanolithography* combined with wet-chemical etching has been used to fabricate metal nanostructures with nanoscale precision and deliberately designed shapes (lines, dots, rings, and triangles).[36] Other methods explored in the literature include on-wire lithography, which merges the template-directed synthesis of nanowires with electrochemical deposition and wet-chemical etching [37] and the combination of ion- and electron-beam techniques to prepare Au micro-hole arrays, grooves and nanowires circuits [38].

b. Chemical methods

The most important characteristic of colloidal chemistry routes is to provide nanoparticles that are soluble in most common polar and non-polar solvents and are very stable against aggregation over time. Surface functionalization of colloidal nanoparticles can be promptly tailored by post-synthetic chemistry depending on their final application. These are important features particularly relevant for achieving cost-effective nanoparticle processing for nanomedicine and optoelectronic devices. Wet chemistry procedures involve the presence of capping agents which provide morphological, compositional and colloidal stability to the metal nanoparticles and assist in the preferential growth of specific facets, (affect the final nanocrystal shape and size), These methods have enabled a variety of non-spherical metal nanoparticles, including rods [39,40] wires, cubes [41], nanocages [42], (multi-) concentric shells [43], triangular prisms [44], hollow tubes, capsules [44], and branched nanocrystals [45]. This rich architectural landscape offers much larger control over the physical properties as compared to spherical materials systems. The resonance frequency is tunable over a wide range from the blue to the near-infrared region.(Figure 6).

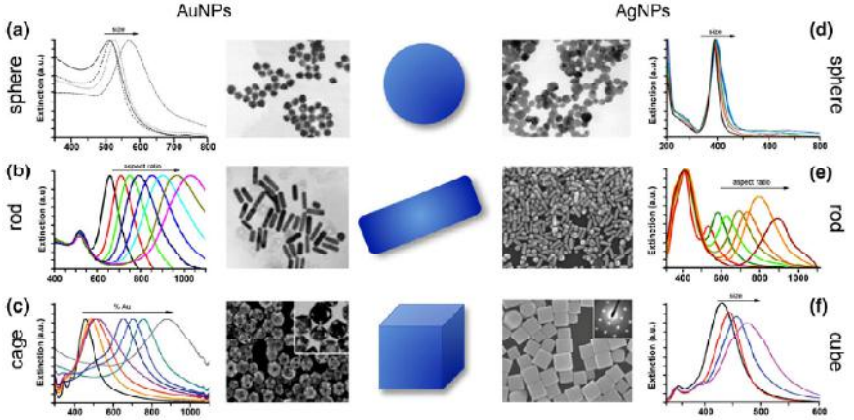

Figure 6: Commonly synthesized Au and Ag nanostructures. Graphical illustrations, electron micrographs and extintion spectra for (**a**) Au nanospheres, (**b**) Au nanorods, (**c**) Au nanocages, (**d**) Ag nanospheres, (**e**) Ag nanorods and (**f**) Ag nanocubes. Observed red-shift in extintion spectra is representative of increasing nanostructure size (**a, d, f**), increasing aspect ratio (**b, e**) and (**c**) increasing Au deposition. Reprinted with permission from ref. [46]

This is particularly important for utility in biological applications where operation in either the 700–900 nm/1000-1300 nm wavelength regions is preferred due to reduced light attenuation caused by both absorption and scattering from tissue constituents (water, lipid, hemoglobin, melanin). This allows significant penetration depths down to the millimetres and centimetres scale which is advantageous [23].

i. Spherical plasmonic nanoparticles

Surface energy minimization favors the formation of spherical objects for larger colloidal nanoparticle [47] Most colloidal routes to Au nanoparticles involve the chemical reduction of Au ions, starting from Turkevich's protocol, the first published method and most widely used to produce Au nanoparticles in aqueous environment.[48] Variation of the citrate/Au ratio enables colloidal particles with diameters ranging from 10 to 150 nm to be generated. For particles larger than 30 nm, the size distribution widens and the ellipticity of the particles significantly exceeds unity. The most popular approach to prepare spherical Au nanoparticles in non-polar solvents is Brust's method, developed in 1994, utilizing a two-phase system where Au ions are reduced by $NaBH_4$ at an oil–water interface. Tetraoctylammonium bromide (TOAB) is used as the phase transfer catalyst and stabilizing agent. Due to the relatively weak binding between TOAB and Au nanoparticles (diameter < 10 nm), alkanethiols are introduced to prevent aggregation [49]. Milder reducers such as sodium citrate yield Au nanoparticles with diameters larger than 10 nm. Spherical Ag nanoparticles are one of the most commonly synthesized Ag nanostructures. In general, the Ag precursor has a reactivity similar to Au salt allowing the Turkevich method to be employed. Larger particle diameters (50–100 nm) are typically obtained when using citrate as the reducing and capping agent.[48] Smaller Ag nanoparticles (5–20 nm) can be obtained when $NaBH_4$ replaces citrate as the reducing agent.[50] More recently, Suzuki and coworkers have described a combined seed and laser technique to produce Ag nanoparticles with diameters ranging from 10–80 nm.[51] Ag colloid seeds with an average diameter of 8–10 nm are produced by the citrate reduction of silver nitrate ($AgNO_3$) followed by irradiation with a second harmonic Nd/YAG laser source (λ = 532 nm)..

ii. Anisotropic plasmonic nanoparticles

Anisotropic plasmonic nanoparticles are more interesting for photothermal and near-infrared applications as the longitudinal plasmon band can be manipulated across the visible to near-infrared region. In order to control the formation of non-spherical Ag and Au nanoparticles, various methodologies have been recently developed including the use of rigid templates, and the use of appropriate capping reagents to kinetically control the growth rates of various facets of a seed. [23] In the latter approach, the template serves as a scaffold where metal is generated in situ, either therein or around it, thus imparting a morphology complementary to the template geometry. A wealth of templates have been successfully developed and utilized, including channels within porous materials, mesoscale structures (including Langmuir films) self-assembled from organic

surfactants or block copolymers, biological macromolecules such as DNA strands or viruses, and existing nanostructures synthesized using other approaches. [40,47,52–56] Templates are also frequently used in combination with photochemistry, electrochemistry, and sonochemistry. It is often necessary to selectively remove the template in order to harvest the prepared nanoparticles.

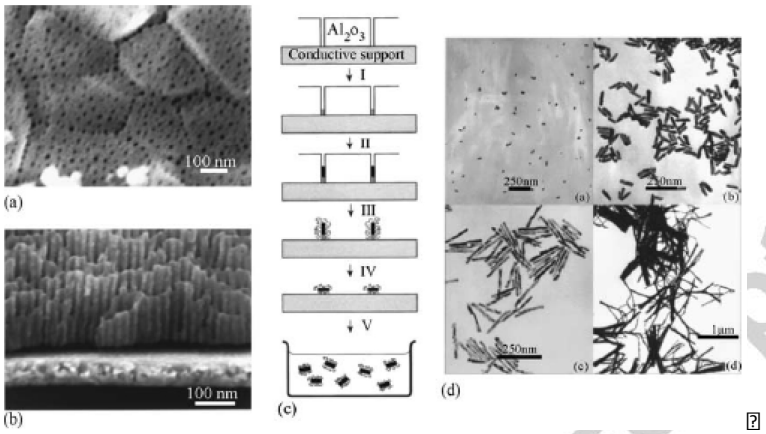

Figure 7: (**a** and **b**) Scanning electron microscope images of an alumina membrane. **(c)** Schematic representation of the successive stages during formation of Au nanorods via the template method. **(d)** Transmission electron microscope micrographs of Au nanorods obtained by the template method. Reprinted with permission from ref. [59]

Nanorods and nanowires with tunable diameters can be prepared by controlling the pore diameter of a porous template and the amount of metal deposited within the pores (Figure 7).[57] Such a strategy is limited to a pre-defined nanoparticle size and shape as well as further post-synthesis functionalization.[58] Self-assemblies of surfactant/aqueous mixtures provide an interesting class of "soft" templates. Surfactant molecules are known to spontaneously organize into micelles in aqueous media (or reverse micelles in organic solvent systems) when their concentration reaches a critical value. Water is readily solubilized in the polar core of reverse micelles, forming a central aqueous environment, which can be utilized as a spatially confined reactor vessel where nanoparticle formation can occur. A variety of synthetic methods differing only in the strategy to trigger Au precursor reduction have been proposed in literature including electrochemical,[60] seed-mediated,[61,62] seedless,[63] photochemical,[64,65] and microwave-assisted approaches.[66] The most widely investigated (and optimized) colloidal approach to Au nanorod synthesis is a seed-mediated growth method was first described by Murphy et al. in 2001 and further explored by Nikoobakt and El-Sayed in 2003.[61,62] This method requires a solution of small seeds (3–5 nm) produced from the reduction of chloroauric acid by $NaBH_4$ in the presence of CTAB (cetyltrimethyl ammonium bromide). Once formed, the seeds are introduced into an Au (I) growth solution containing ascorbic acid, $AgNO_3$ and CTAB. (Figure 8)

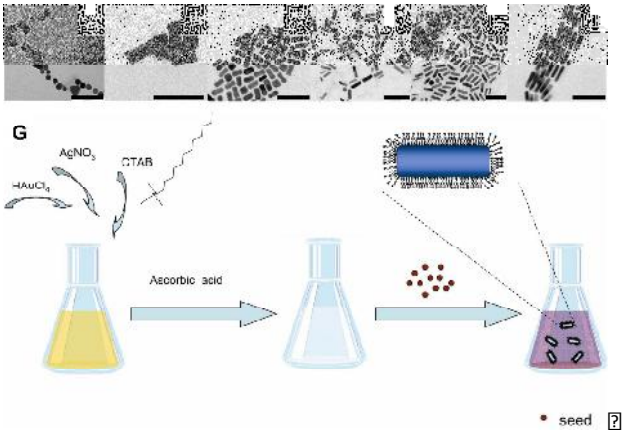

Figure 8: Transmission electron microscope images of Au nanoparticles **(A)** and Au nanorods with increasing aspect ratio **(B–F)**; scale bar 100 nm. (**G**) General scheme of the synthetic steps in seed-mediated growth of Au nanorods assisted by Ag ions.

The seeds serve as nucleation sites for the anisotropic reduction of Au+ while the transverse diameter is relatively constant at 15 nm, the length (and thus aspect ratio) of the nanorods can be adjusted by controlling pH [67] and controlling the relative concentration between o $AgNO_3$ and Au precursor (Figure 8) [65]. In addition to their ability to form micelles, surfactant molecules can also bind preferentially to specific crystal faces and direct NC growth.[68] Competitive binding events of CTAB was shown by Murphy to lead to the generation of faceted spheres which can be further processed into 1D nanostructures.[69] Different surfactants can be used in combination with CTAB to vary the aspect ratio of the nanorods produced by this technique.[62] Factors including the surfactant head group and chain length affect the final characteristics of the structures formed. Alkyltrimethylammonium bromides are the most popular choice having been used to demonstrate a variety of different sized rods. .[61] The variation of hydrocarbon tail length in tetraalkylammonium surfactants (C_nTAB) results in a surprisingly strong dependence of aspect ratio.[70]. Interestingly, impurities in the various commercial CTAB sources greatly affect the yield, dispersity, and aspect ratio.[71] and, in general, the growth mechanism of Au nanorods is still unclear although numerous theories about controlling variables exist in the literature. These include the preferential binding of the head group of a cationic surfactant to the {100} face rather than to the less-favored rod end [68,72], the influence of the CTAB double layer electric field,[73] the interaction of CTAB counter ion (i.e. Br^-) [74] and the crucial role of small amounts of Ag^+ [75–77] Interestingly, varying the ratio between Ag and Au concentration, the aspect ratio of the nanorod and its crystal structure. 65] The underpotential deposition of Ag onto the Au nanorod, that is electrodeposition of the metal Ag ion onto the Au nanorod metal surface at a potential less negative than its reduction equilibrium

(Nernst) potential, has been invoked to explain the dramatic role of Ag+ on the growth of the Au nanorods.[75] Indeed, due to the different surface energy of Au facet, Ag deposition on the {110} side of the rod is faster than on the {100} ends, and consequently seeds grow into rods. Accordingly, EXAFS analyses demonstrated that Ag(0) islands are present at the long side of the Au nanorods (i.e. {100} and {110} facets).[65,76] The seed-mediated synthetic scheme used for Au nanorods has been modified by Jana et al. to prepare Ag nanorods with controllable aspect ratios.[61] Silver seeds with a diameter of 4 nm are obtained from the $NaBH_4$ reduction of $AgNO_3$ in an aqueous citrate solution. $AgNO_3$ is then reduced by ascorbic acid in a solution containing these silver seeds, cationic surfactant CTAB, and sodium hydroxide (NaOH). Larger aspect ratios are achieved when the amount of silver seeds present in the growth solution decreases. More recently, Mahmoud et al.[78] synthesized Ag nanorods with different aspect ratios using a polyol reduction method at high temperatures and high stirring speeds..

iii. Plamonic nanoparticles with exotic geometry

Increasing levels of complexity in nanoparticle shape have been reached including two-dimensional (2D), 3D, and branched structures and an extrapolation to hollow structures. High-index concave cubic Au nanocrystals,[79] bipyramids,[75] nanocages,[80] nanocubes,[81] hollow Au nanoshells,[82] and branched nanoparticles [83] including monopods, bipods, tripods, tetrapods, hexapods,[84] and multipods including nanoflowers, nanostars, and urchins have all been demonstrated [85] (Figure 9). Branched nanoparticles are highly desired because of their sharp edges and the correspondingly high localization of surface plasmon modes. There are great expectations for such branched Au nanoparticles as potential candidates in nanocircuits and nanodevices, and for *in vivo* applications.[86] (Baffou et al. investigated quantitatively the heating efficiency of different Au nanostructures used in plasmonic heating applications [87,88]. Interestingly, small, flat, elongated, or sharp nanoparticles are more efficient heaters than larger nanostructures. The red-shift of the plasmon resonance occurs with a substantial increase in the heating efficiency as the aspect ratio of the rods is increased. These effects come from the fact that the incoming electric field penetrate more easily inside the thin nanostructures making the whole amount of Au matter heat source.[89]

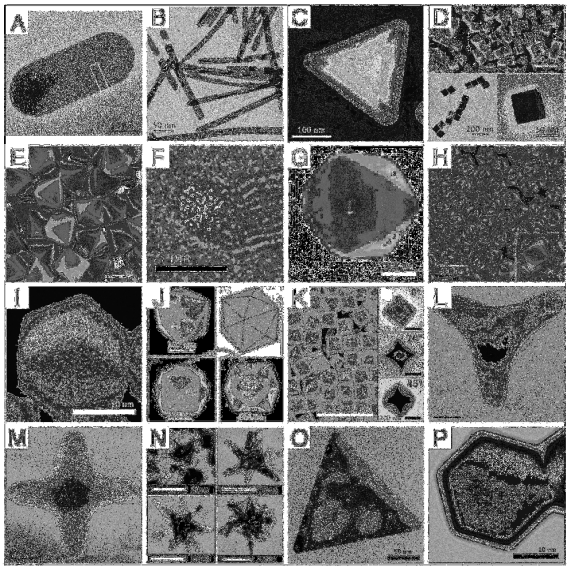

Figure 9: The major classes of noble metal nanoparticles shapes seen through transmission electron microscope and/or scanning electron microscope: (**A**) Au octagonal single-crystal rod, (**B**) Au pentagonally twinned rods, (**C**) Au tetrahedron nanoparticles, (**D**) Pd hexahedron (i.e., cube) nanoparticles, (**E**) Au octahedron nanoparticles, (**F**) decahedron, (**G**) Au icosahedron nanoparticles, (**H**) Au trisoctahedron nanoparticles, (**I**) Au rhombic dodecahedron nanoparticles, (**J**) Pt tetrahexahedron nanoparticles, (**K**) Au concave hexahedron nanoparticles, (**L**) Au tripod nanoparticles, (**M**) Au tetrapod nanoparticles, (**N**) Au star nanoparticles, (**O**) Au triangular plate/prism nanoparticles, and (**P**) Au hexagonal plate/prism nanoparticles. Reprinted with permission from ref. [90]

Au nanoshells ,composed of dielectric cores (typically SiO_2) coated with thin metal layer(s) (such as Au), are also very interesting. Although they exhibit a single LPR similar to spherical nanoparticles, it can be tuned across the visible and infrared region over a range of wavelengths spanning hundreds of nanometers, far exceeding the spectral range of spherical particles.[91] Silica nanospheres are the most successful templating nanomaterial. The size and the thickness of the Au nanoshells can be controlled as a function of reaction time and concentration of the plating solution (Figure 10A,B).[92] More exotic "nanomatryoshka" live structures, consisting of a solid Au core surrounded by a thin dielectric (SiO_2) layer capped with an outer Au shell layer, have been reported in literature. The resulting plasmonic properties arise from the strong interaction between the plasmon modes of the Au core and shell, resulting in hybridized modes that can be tuned into the near-infrared (Figure 10 C,D).[93] More complex nanostructures, grown utilizing Au nanodisks as a core, incorporated the subsequent growth of Ag around a Au core (by galvanic replacement) have been shown. The number of shells was tuned by controlling the total number of Ag-shell-growth and galvanic-replacement reaction steps. The gap distance was controlled by tuning the thickness of the Ag layer grown on the Au nanoplate (Figure 10 E, F).[94]

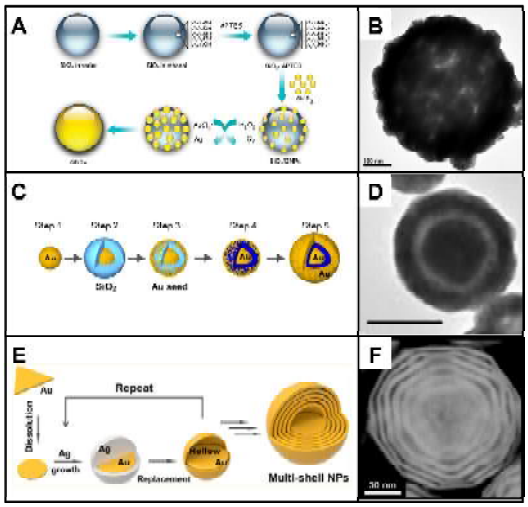

Figure 10: (**A, B**) Schematic representation of Au nanoshell synthesis and representative transmission electron microscope image. [reprinted with permission from ref [95,96] (**C, D**) Schematic representation of Au nanomatrioska synthesis and representative transmission electron microscope image (scale bar 50 nm) [reprinted with permission from [93] (**E, F**) Schematic representation of Au multishell synthesis and representative transmission electron microscope image. Reprinted with permission from ref. [94]

iv. Metal nanoparticles dimers and trimers

When metal nanoparticles are placed adjacent to each other, their localized surface plasmons can couple. The local electric field enhancement in the gap region of these plasmon-coupled metal nanoparticles is usually much larger than that associated with isolated nanoparticles. This coupling e has been employed for enhancing optical signals [97], second-harmonic signals,[98] two-photon photoluminescence,[99] and in nanometric optical tweezers[100]. Closely spaced nanoparticles, in particular, nanorods, can function as optical nanoantennas to link propagating radiation with confined optical fields.[101] Chains of structures can act as subwavelength waveguides for use in integrated photonic circuits.[102] This coupling is usually accompanied with large shifts in the extinction or scattering of specific spectral peaks which can be exploited in biomedical applications.[103,104] Au nanoparticle dimer, trimer, and tetramer structures have been fabricated by electron beam lithography,[105,106] DNA interactions,[107] organic-bridged ligands,[108] polymer lamellar single crystals,[109] and solid-phase mono- and asymmetric-functionalization [110,111]. Formation of aggregate micelles containing two or three spherical Au nanoparticles utilizing a block copolymer microemulsion has been reported.[112]

Nanoparticle aggregates can be obtained by controlling aggregation kinetics. The general difficulty in this methodology is that if the interactions between nanoparticles are too weak, then their assembly may be lost during purification. If the interactions are too strong, then further

aggregation may occur when the sample is concentrated or purified.[108] Putting shells on nanoparticles can help by preventing the dissociation of nanoparticles while guarding against further aggregation. For instance, the well-known tendency of silica to form ordered colloid crystals have been exploited to create 2D and 3D arrays to obtain homogeneous optical metamaterials where plasmonic nanoparticles are separated by the silica shell.[113] More importantly, the silica shell can provide a versatile platform for functionalization opening up a wide range of properties for biomedical application. It is possible to selectively obtain Au nanoparticle dimers and trimers embedded in silica beads[114,115] by controlling the growth conditions. The density of the ligand agent coordinating Au nanoparticles surface was found to be a crucial parameter in controlling both the morphology and multiplicity of the metal core inside each silica shell.[114] (Figure 11).

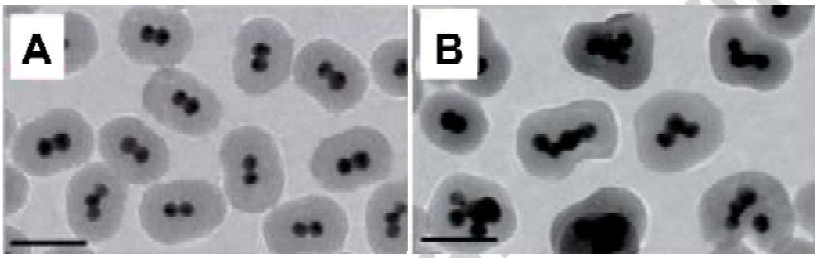

Figure 11. Transmission electron microscope images of dimers (**A**) and trimers (**B**) of core–shell silica coated Au nanoparticles. Adapted with permission from ref. [114].

4. Integration in functional structure and devices

The ability of integrating single and coupled nanoparticles or nanostructures in functional plasmonic architectures and devices enables both fundamental studies and an exploration in a variety of optoelectronic devices due to an ability to concentrate, guide, and switch light on the nanoscale. As stated, these plasmonic structures can be fabricated starting from a defined number chemical or physical methods. Critical prerequisites are the rational design of the building blocks, and the production of high-quality metallic nanoparticles with tunable size and controllable shapes. The field of nanoplasmonics has greatly benefited from substantial recent progress in the synthesis of metal nanoparticles by means of colloidal chemistry. The following section describes different strategies post-synthesis to process and functionalize nanoparticles toward specific biorelated applications and integration in devices.

a. Functionalization

Wet chemistry procedures leave a capping agent which as explained drives morphological, compositional and colloidal stability to the Au nanoparticles. The capping agent can be replaced by post-synthesis treatments with other molecules having higher compatibility with the polymer matrix. The capping exchange with a new ligand can occur either by mass action or by using functional groups with a stronger affinity for the nanoparticle surface.. The new ligand can be bifunctional carrying, having a strong affinity for the nanoparticle surface from one end and a different affinity (and functionalization/chemistry) on the other end Alternatively, the new capping agent can simply differ from the original one through the length of the alkyl chain. Different types of nanoparticle functionalization procedures will be summarized and briefly illustrated with relevant examples. Nanoparticle functionalization can occur by means of noncovalent modifications such as electrostatic interactions, hydrophobic entrapment, and van der Waals forces, in addition to covalent modifications through a variety of chemistries.[116,117]

i. Functionalization for biorelated applications

One of the most critical requirements for use of Au and Ag nanostructures in biomedical and nano-electronic applications is their stability against aggregation. Suitable tailoring of a nanoparticle surface can also make them compatible with a biological environment, thus fostering their use for biomedical applications. Surface treatment steps enabling building blocks that can effectively and safely bind to biological moieties for bioconjugation will be briefly reviewed. As they do not depend on harsh chemicals, electrostatic interactions, have been extensively used to functionalize Au and Ag nanoparticles to biomolecules including DNA, peptides, and antibodies. This method relies on the attraction between two oppositely charged species including the the nanoparticle surface and a (bio)molecule of interest (Figure 12-DNA)) [118] or a specific antibodiy to selectively target and photothermally destroy cancer cells,[119] or selectively detect a specific analyte.[120]

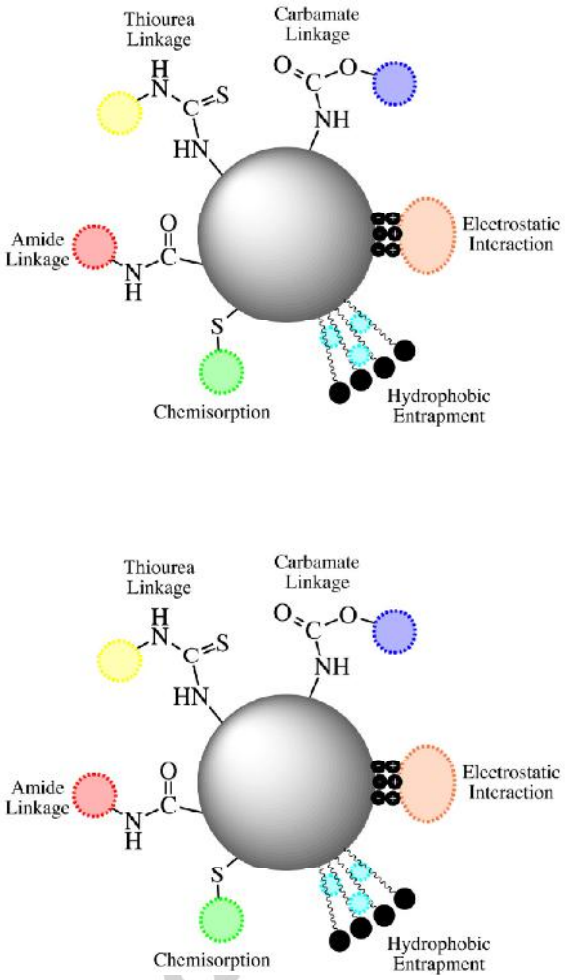

Figure 12: Common functionalization strategies for Au and Ag nanostructures. Reprinted with permission from ref. [46]

Rotello and co-workers exploited non-covalent interactions to successfully load hydrophobic therapeutics, tamoxifen, and β- lapachone, onto Au nanoparticles.[121] The Au nanoparticles were designed to mimic micelle structures (i.e., a hydrophobic interior and a hydrophilic exterior) which allowed for the encapsulation of hydrophobic drugs in the hydrophobic pockets. Covalent interactions generally provide greater stability and reproducibility of molecular functionalization (Figure 12). Chemisorption bonding, is commonly used to attach thiol-terminated (bio)molecules and (bio)polymers to nanoparticle surfaces through strong metal-S bonds. THE bond energy between Au and S is 44 kcal mol^{-1}.[122], achieved when A sulfur atom donates a lone pair of electrons to the empty orbitals of Au or Ag atoms at an interface.[123] Thiolated biopolymers such as (poly(ethylene glycol) and polyoxazoline (POx) have been anchored to Au nanoparticles surfaces using this bond type to enhance nanoparticle stability in physiological environments as well as preventing nonspecific binding of serum proteins and opsonization when introduced into *in*

vivo systems.[124,125] Other biocompatible polymers used for physiological nanoparticle stabilization include polyvinylpyrrolidone (PVP), poly(styrene sulfonate) (PSS), and poly(lysine) (PLL).

Metal-S bond formation has also been utilized to adhere oligonucleotides to Au and Ag nanoparticle surfaces,[126,127] arginine–glycine–aspartic acid (RGD) and nuclear localizing signal (*nanosphere lithography*) peptides [128].. Many nanoparticle conjugate systems utilize bifunctionalized linkers to covalently attach therapeutic drugs and biomolecules due to the reduction of undesirable structural changes that arise from direct interaction. Commonly used linkers for biomedical applications include oligoethylene glycol (OEG) and (poly(ethylene glycol) polymers modified with amine ($–NH_3^+$), carboxyl ($–COO^–$), isothiocyanate (–N=C=S), or maleimide ($H_2C_2(CO)_2NH$) functional groups. These functional groups allow for conventional coupling strategies, such as carbodiimide-mediated esterification and amidation.[129] (Figure 12) Tumor-targeting antibodies have been conjugated to nanoparticles using heterobifunctional (poly(ethylene glycol) linkers and EDC/NHS coupling (1-Ethyl-3-(3-dimethylaminopropyl)carbodiimide; N-hydroxysulfosuccinimide).[130] Click chemistry, most notably azide-alkyne Huisgen cycloaddition, which involves the use of a Cu catalyst, has also been utilized for nanoparticle functionalization.[46,131]

ii. Functionalization toward integration in devices

Polymer thin films containing metal nanoparticles are of growing interest in photovoltaics, nanoelectronics, and optics.[132–134] Compatibility of metal nanoparticles with organic polymers usually starts by considering suitable solvents (often apolar solvents). Protocols for spherical Au nanoparticles in apolar solvent are numerous and include the use of stabilizers including thiols,[49] phosphines,[135] amines,[136] chalcogenides,[137] carboxylates,[138] and polymers,[139] More challenging is the synthesis of anisotropic metal nanoparticles in organic solvents. Phase transfer of metal nanorods prepared in water assisted by proper surface functionalization is a convenient route to enabling anisotropic metal nanoparticles in different non-polar host matrices. Proper surface functionalization can prevent nanoparticle aggregation and consequently localized plasmonic resonance shift. Different approaches for either complete[140] or partial surface functionalization [141–143] exist for anisotropic systems. For CTAB-capped Au nanorods, the presence of a surfactant bilayer poses a major obstacles it is highly packed. Molecules containing functional group with strong affinity for metal surfaces including cyano (–CN), mercapto (–SH), carboxylic acid (–COOH) and amino ($–NH_2$) groups can be effectively used to at partially displace the original

bilayer.[139,144] Alkylamine and alkylthiol groups have been shown to effectively replace the native capping ligand and to allow nanoparticle incorporation in host polymer films.[145,146] Combinations of covalent and electrostatic interactions can be used to promote the phase transfer of hydrophilic metal nanoparticles into an organic solvent for further incorporation. Mercapto-acids can interact with a NC(what is NC) surface through thiol groups while the outermost exposed carboxylic moiety can be charged for electrostatic interaction.[147,148] As an example mercaptosuccinic acid (MSA) has been anchored to Au nanoparticle surface while leaving the two carboxylic groups free to electrostatically interact with organic soluble cationic surfactants (e.g. tetraoctylammonium bromide (TOAB) dissolved in toluene). Such a functionalization allows Au nanoparticles to phase transfer from water to toluene while retaining their original properties. ,.[133,149] Au nanorods have been also successfully extracted into chloroform by exploiting decanoic acid. Deprotonated carboxylic terminal groups electrostatically bind the positively charged CTAB bilayer, while the alkyl chain provides good dispersion capability in organic solvents, (i.e. nanorod dispersions in liquid crystals (Figure 13).[148]

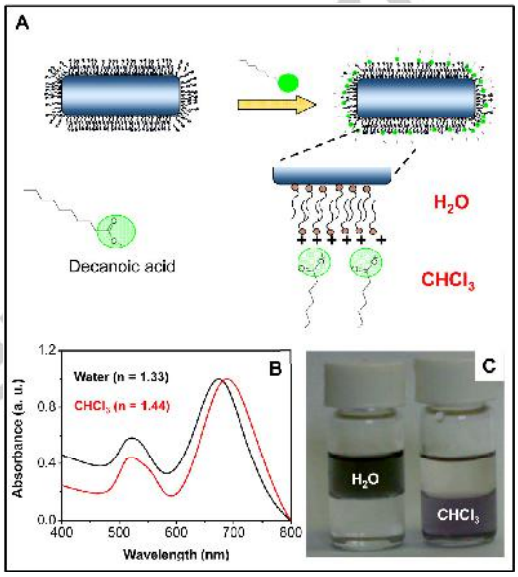

Figure 13: (**A**) Sketch of the decanoic ligand exchange procedure carried out on water soluble Au nanorods. (**B**) Absorption spectra and (**C**) picture of vials of Au nanorods in different solvents. Adapted with permission from ref. [148]

Nanoparticle based architectures

In this section a few of the main methods for the fabrication of plasmonic architectures will be described. Plasmonic structures can be constructed from precise numbers of well-defined metal nanoparticles that are held together with molecular linkers, templates or spacers. Control of the resulting plasmonic properties can be achieved not only by tuning the size and shape of individual nanoparticles, but also by changing the number of nanoparticles in the assembly, by varying the directionality of nanoparticle organization, and by fine tuning the interparticle distance. Manufacturing of plasmonic architectures has been addressed by a variety of methods. Electron beam lithography has been widely explored, even though a wide range of limitations (throughput, area) exist. Solution-based nanoparticle organization procedures offer numerous advantages including the ability to reduce interparticle distances enabling the fabrication of highly complex nanoparticle ensembles with a hierarchical order. Noble metal nanoparticles (e.g. Au and Ag) with controlled geometry can be considered ideal 'atoms' for introduction into metamaterial architectures. Careful adjustment of nanoscale forces acting on individual nanoparticles in solution, use of various types of templates, and application of external fields (magnetic, electric, or flow fields, as well as by capillary forces) are crucial to achieve plasmonic nanostructured materials with tunable optoelectronic and thermal properties. Assembly in solution offers principle most simple, the most straightforward yet diverse approach. In this perspective, the selection of a suitable type of ligand discussed in the previous section, drives the nature of nanoscale forces leading to diverse nanoparticle architecture formations. Plasmonic architectures fabricated using solution methods will be described.

i. Clusters and 1D nanoparticle assembly in solution.

Preparation of 1D assemblies of nanoparticles represents a challenge that has been examined with a set of very diverse strategies all with a goal of providing an effective toolbox for careful engineering of the optical and thermodynamical properties. Dujardin and co-workers [150] reported the fabrication of complex and extended networks of interconnected chains of Au nanoparticles by a spontaneous one-pot self-assembly process driven by interparticle dipolar interactions. The superstructures formed exhibited an overall globular size of typically 23 μm, built upon individual chain segments which were single particle and 12 nm wide. These particle assemblies enable the fine modulation of the spatial distribution of the electromagnetic field intensity. (Figure 14)

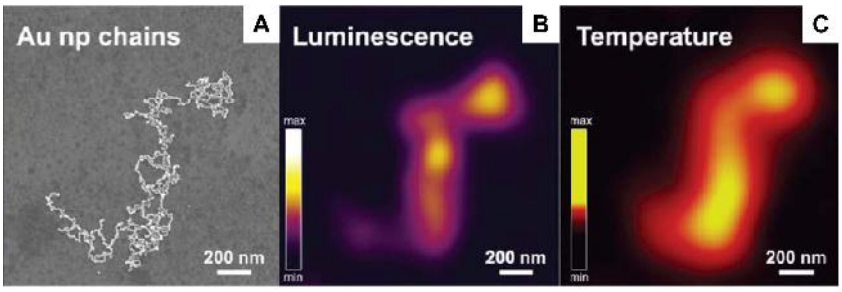

Figure 14: **(A)** Scanning electron microscope image of a small plasmonic nanoparticle networks deposited on ITO/glass substrate. **(B)** TPL and **(C)** Temperature images of the same plasmonic nanoparticle networks for light and heat concentration excited at 730 nm. Adapted with permission from ref. [150]

The self-assembly of these plasmonic nanoparticles network were performed at room temperature by adding 2-mercaptoethanol to a Au nanoparticles solution and was following progress by monitoring the color change from pink to purple as the coupled modes emerge. The optical absorption spectra of these superstructures display both a transverse plasmon mode (520 nm) due to single nanoparticles and a lower energy mode (700 nm) associated with chains of Au nanoparticles where a strong coupling of surface plasmons between neighboring nanoparticles takes place. These longitudinal absorption bands efficiently confine light fields and concentrate heat in the vicinity of these plasmonic chain networks. The planar spatial distribution of the optical field intensity in such superstructures can also be tuned by controlling the linear polarization of the incident optical excitation. Au nanoparticles have been also directly "copolymerized" into chains by using empty polystyrene-block-poly(acrylic acid) block copolymer (PSPAA) templates.[151] Short PAA blocks in an amphiphilic block copolymer were used to promote the reorganization of tan amphiphilic copolymer in the a micelle geometry. The reaction time, acid quantity, and the Au nanoparticle/PSPAA micelles concentration ratio was found crucial in controlling the sphere to cylinder vesicle conversion which gives rise to various random "copolymers". The ability to include small Au nanoparticles (d = 16 nm), large Au nanoparticles (d = 32 nm), and Au nanorods provides a convenient and general approach for assembling nanoparticles into long-chain structures. Au nanorods, along with nanoparticles with a more complex geometry such as branched shapes, have been organized in superstructures by assembly at the interface between polar and nonpolar solvents followed by transfer onto a glass slide [152, 153]. Characterization of the optical transmission and reflection spectra revealed that layers consisting of Au nanorods exhibit an optical response typical of an effective medium with high specular reflection and a strong red-shifted localized plasmonic resonance response. Layers of branched Au nanoparticles show a more complex response, characterized by a strong decrease in the reflectivity attributed to both light trapping and multiple scattering within the nanoparticle layer. The results suggest at the optical

wavelength scale, the plasmonic mode structure is homogeneous and could potentially be investigated for applications such as surface-enhanced Raman spectroscopy or refractive index sensing. Controlled aggregation of Au nanorods has also been successfully achieved through phospholipid encapsulation [154]. The end-functionalization of nanorods with polymers enables an end-to-end self-assembly of nanorod chains and control over the inter-rod separation through the molecular weight of the polymer linker. Phospholipid encapsulation has been found effective in reducing the polydispersity of the aggregates and making themwater dispersible. These features along with the preferential isolation of nanorods short-chain have been found relevant for maximizing surface-enhanced Raman spectroscopy, making these structures promising optical probes for biological applications. Another simple and versatile light-based strategy developed to grow low dimensional Au superstructures utilizes prolonged UV irradiation of TiO_2 nanorod-stabilized Au nanoparticles in organic media. A progressive formation of distinctive chain-like assemblies linking segments of a few Au nanoparticles, together over areas of about 500 nm2 has been reported ([155]).

ii. 2/3 D self-assembly in solution

Moving towards 2 and 3 dimensional assemblies and lattices, self-assembly also represents a particularly simple and effective strategy. Such approaches rely on a delicate equilibrium of specific short-range interactions, including dipolar forces and van der Waals interactions. It is generally accepted that minimization of free energy contributions is the driving force behind superstructure formation. Spontaneous organization requires control of nanoparticle size and distribution in addition to nanoparticle concentration, dispersing solvent, and substrate. The capping agent chain length and composition can also strongly affect the final geometry for a binary superlattice.. Corricelli et al [156] showed Au nanoparticles can self-assemble by means of a simple solvent evaporation strategy into a two-dimensional (2D) superlattice with a controlled geometry and extending over large area using drop casting onto a functionalized silicon substrate. The substrate surface chemistry is important to the self-assembly as indicated by structural and morphological investigation. Spectroscopic ellipsometry indicated that the plasmonic properties strongly depend on nanoparticle ordering and mutual near-field interactions. Attractive interparticle forces drive, in poor solvents, the self-assembly of Au nanoparticles coated with polymer ligands which are able to effectively coordinate the nanoparticle surface with suitable functional groups. The occurrence of a solvophobic force induces nanoparticle clustering to minimize surface energy by shielding negative interactions between the polymer ligand and solvents. This strategy has been effectively

used for plasmonic spherical nanoparticle and Au nanorods, stabilized with polystyrene, polyvinyl carbazole and poly(N-isopropyl acrylamide).[153]

iii. 3D self-assembly of nanorods

Nearly perfect three-dimensional assemblies of Au nanorods which exhibit plasmonic antennae enhancement of electrical fields have made the fast and direct detection of prions in complex biological media possible. These systems have also been demonstrated as excellent surface enhanced Raman scattering spectroscopy substrates exhibiting uniform electric field enhancement, leading to reproducibly high enhancement factors in the desired spectral range. Au nanorods (75 × 25 nm; aspect ratio 3) were made using the seed mediated method adapted to obtain high yield and very narrow size distributions ($\sigma \sim 3\%$). These were crystallized into 3D colloidal crystals (supercrystals) arranged as individual islands of uniform dimension through slow drying of the aqueous Au nanorod dispersions in a humid atmosphere. Both the diameter and height of individual nanorod islands were approximately 1 μm which corresponds to approximately 15 layers of nanorods perpendicular to the substrate.[157] Highly organized supercrystals of Au nanorods have been vertically aligned as microplates over a large area through self-assembly from a bulk solution evaporation method. This evaporative self-assembly strategy is based on the continuous movement of the contact line (coffee ring effect). As a result, it is possible to obtain a uniform deposition of Au nanorod superstructures over a large area, with the formation of Au nanorod supercrystals with geometrically symmetric shapes (Figure 15). [158] The self-assembly of colloidal metal nanoparticles based on the interactions between molecules located at the nanocrystal surfaces has proven the most effective approach toward controlling nanoparticle spacing in 3D substrates.

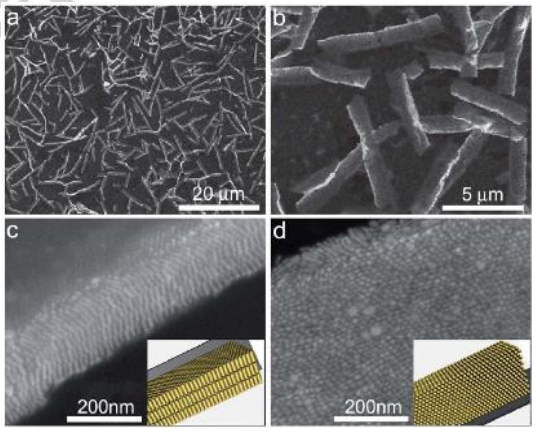

Figure 15: (**a** and **b**) Scanning electron microscope images of vertically aligned, supercrystalline Au nanorods assembly in microplates nanorod ([Au nanorods] = 8 nM, [CTAB] = 1 mM). (**c**) Scanning electron microscope image of an upstanding microplate showing the lying nanorods aligned in a smectic way. (**d**) Scanning electron microscope image of a tilted microplate showing the hexagonally packed, standing nanorods. **Insets** of (**c**) and (**d**) are the related 3D

simulation models of the supercrystalline microplates viewed along different observation angles. Reprinted with permission from ref. [158]

A straightforward approach to obtaining long-range plasmonic supercrystals made of standing core-shell Au-Ag nanorods (Au@Ag nanorods), stabilized with gemini surfactants was reported by controlling drop casting conditions. Replacing Au with Ag and/or by refining substrate production.[159] can be used to improve optical sensors based on SERS. The Langmuir-Schaefer technique has proven effective for assembling meta-atoms of silica-coated Ag nanoparticles into thin films of large area and well-controlled thickness. The silica shells ensure a constant distance between the silver cores providing coupling of the LPR in the assembled composite material. The optical response was studied by normal angle spectral reflectance measurements and variable angle spectroscopic ellipsometry and examined theoretically using numerical simulation tools.[160] Metal nanoparticles have also been successfully assembled using a microfluidic evaporation technique to fabricate high diffraction materials. The technique enables fabrication of three-dimensional bulk samples consisting of a large number of layers (>600) from a suspension of nanoparticles. spectroscopic ellipsometry was used to characterize the optical properties. The technique reduces complexity and costs in assembling plasmonic materials enabling a pathway to engineering optical devices including lenses, filters and modulators by selecting nanoparticles with suitable characteristics.[113] A similar convective assisted capillary force assembly (CA-CFA) method was demonstrated in the fabrication of micrometer-sized assemblies of arbitrary footprint (e.g., square, four branched-star, triangle, or disk) from a suspension of monodisperse Au nanoparticles. (Figure 16)

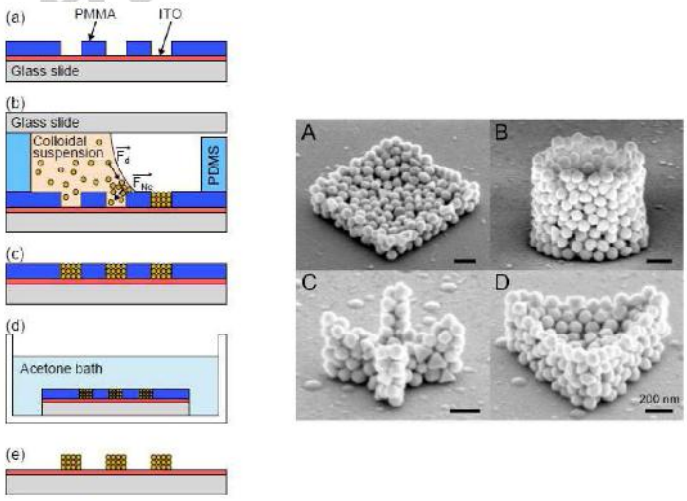

Figure 16: **(Left)** 3D structure fabrication process: **(a)** preparation of the assembly substrate by e-beam lithography of a PMMA substrate layer deposited on an ITO-coated glass slide, **(b)** CA-CFA of the colloidal suspension by controlled

evaporation in a microfluidic cell, **(c)** assembled sample after total evaporation, **(d)** removal of the PMMA resist by immersion in an acetone bath, **(e)** resulting 3D metallic structures made of colloidal gold particles. **(Right)** Four scanning electron microscope images of nanoparticle architecture assemblies realized with 100 nm ± 5 nm gold particles. The typical height of the superstructures is 250 **(A)**, 490 (**C** and **D**), and 950 nm (**B**). Reprinted with permission from ref. [161]

The structures were prepared using a substrate on which 100-nm diameter Au colloids were assembled by CA-CFA. The control parameters (e.g. temperature and humidity) allow a controlled evaporation rate and the hydrodynamic drag force F_d confines the nanoparticles at the air−liquid−solid contact line. In a second step, the nanoparticles are pushed into the cavities by capillary forces. These composite objects sustain specific plasmon modes depending on their shape and coupling between the Au nanoparticles. The small interparticle distances enable strong electromagnetic coupling which delocalize the modes over the structure. Electrodynamic calculations confirming the physical properties of this plasmonic modal shaping has fostered interest in using such assemblies as ultracompact opto-electronic devices,. Porous structures like these are ideally suited to increase the interaction between light and photoactive molecules. This novel CA-CFA assembly method paves the way for fabricating other interesting plasmonic structures including chiral nanostructures or left-handed materials.(Figure 16).[161]

iv. Electrostatically mediated assembly.

Self-assembly of plasmonic nanoparticles can be also be induced by attraction forces including electrostatic interactions. Layer-by-layer assembly, based on electrostatic interactions among the components, results in a stacked structure of alternating positively and negatively charged materials. This approach is particularly cost-effective and versatile allowing large flexibility in the chemical nature of the components, the number of layers, and the layering sequence. Nanostructured films based on Au nanoparticles including nanorods and polyelectrolytes have been obtained using this assembly technique. The morphology and plasmonic features depend on the nature of the anchoring polyelectrolyte on the substrate, the number of layers, and the type of nanoparticle mutual assembly. Charge transport through nanorod-multilayer films has been reported generating interest as photoelectrochemical sensors including a wide variety of materials including organic, inorganic and a variety of biomolecules can be effectively incorporated in multilayered architectures.[162]

v. Bio-specific interactions

Bio-specific interactions offer a wide functionalization platform for metal nanoparticles. One of the most investigated strategies is the assembly of metal nanoparticles stabilized with DNA ligands. Since 1996, plasmonic structures driven by DNA interactions have been utilized. DNA has been used to fabricate regularly arranged nanoparticle chains (plasmonic polymers) and extended two- and three-dimensional ordered arrays (plasmonic crystals). DNA and peptide-directed assemblies have also proved to be viable methods for the controlled arrangement of metal nanoparticles in chiral geometries.[163] DNA origami enables the high-yield production of plasmonic structures that contain nanoparticles arranged in nanometer helices. Circular dichroism effects in the visible spectrum have been demonstrated due to the chiral morphology of organic molecules and the plasmonic properties of nanoparticles. Chiral materials composed of organized nanoparticle superstructures have promising applications in photonics particularly as metamaterial-based sensing platforms. The design and realization of a three-dimensional (3D) hierarchical architecture for utility as a SERS-based immunosensor for protein biomarker detection was demonstrated.[164] Antibody molecules are immobilized on a plasmonic Au triangle nanoarray pattern while the detection antibody molecules were linked to the Au nanostar@Raman reporter@silica sandwich nanoparticles. When protein biomarkers are present, the sandwich nanoparticles are captured over the gold triangle nanoarray, forming a confined 3D plasmonic field, leading to the enhanced electromagnetic field in intensity and in 3D space. The Raman reporter molecules were exposed to a high density of "hot spots" which results in the amplification of the Raman signal.. This SERS-based immunosensor exhibits a wide linear range and a low limit of detection toward human immunoglobulin G protein. It has been demonstrated successfully for detection of vascular endothelial growth factor in human blood plasma from clinical breast cancer patient samples.

c. Processing for integration in device

Plasmonic nanostructures access a wide range of plasmonic properties making them potentially useful in a variety of devices. The next step after their synthesis and functionalization is integration into devices. Incorporation of Au nanoparticles in a polymer matrix represents one of the most straightforward (and growing) approaches. Au nanoparticles embedded in optically transparent polymer exhibit high optical absorption and thermal response suitable for biomedical and optoelectronic applications. Resonant irradiation of Au nanoparticles deposited in polymer films allows localized control of the optical and thermal energy for photovoltaic, sensing, optoelectronic, and catalytic applications.[132] Thermoplasmonic transport in Au nanoparticle–PDMS thin films

was recently demonstrated. The measured thermal emission and dynamics of Au nanoparticle–PDMS thin films exceeding expected values obtained by finite element analysis including Mie absorption, Fourier heat conduction, Rayleigh convection, and Stefan–Boltzmann radiation. Refractive-index experiments and temperature profiles indicated light was internally reflected and power was dissipated transverse to the film surface. This enhanced thermoplasmonic dissipation are interesting with respect to the opto and bioelectronic application of these systems.[132] The combination of Au with a polymer binder was utilized to achieve an adaptive material enabling significant and reversible tuning of the plasmonic properties. The use of a responsive polymer, poly(4-vinylpyridine) (P_4VP) was found to drive the reversible breaking and reconstruction of linear and branched chains of Au nanoparticles adsorbed on an ultrathin (1 nm) film as a function of pH. Below the isoelectric point, the polymer chains are extended and the Au nanoparticles adsorbed on the polymer layer can be considered as individual nanoparticles. At higher pH, the polymer chains collapse into a globule state which causes the nanoparticles to interact with each other giving rise to strong interparticle plasmon coupling. This reversible aggregation results in large and reversible modulation of the optical properties exhibited by the assemblies.[165]

PDMS as a host matrix for Au nanoparticles has been used to achieve a flexible nanocomposite used in the fabrication of a metamaterial. A wet chemistry approach allowed the design and fabrication of a soft, bulk nanocomposite material which exhibits nonconventional electromagnetic properties in the range of visible light. This work demonstrates the importance of the surface chemistry, as the presence of a double bond in the aliphatic chain of capping agent oleic acid, does not inhibit the crosslinking process in the host PDMS under the typical curing conditions. Instead the ligand is able to contribute successful the PDMS curing, promoting crosslinking, and ultimately promoting nanoparticles and quantum dot incorporation into the polymer. Coherent interactions between quantum dots and plasmonic Au nanoparticles embedded in these PDMS films lead to enhancement of the absorption cross-section of the quantum dots, remarkably modifying the optical response of the entire system. Optical and time resolved spectroscopy studies revealed an active gain-plasmon feedback behind the super-absorption effect.[166] Insertion of an Au nanoparticles/polystyrene layer between the indium tin oxide (ITO) and the photoactive polymer by spin-coating was found to improve the photovoltaic effect of solar cells significantly. Polystyrene was added to improve the film forming properties. Improvement of the device performance is due to good transmission, high work function, good conductivity, and an ultra-smooth surface roughness of the Au nanoparticle layer. These films are a promising buffer layer to facilitate hole collection

from a polymer donor towards an ITO anode in a polymer solar cell.[167] Au nanoparticles have been directly incorporated into the active layer of polymer solar cells based on the donor (poly[2,7-(9,9-dioctylfluorene)-alt-2-((4-(diphenylamino) phenyl)thiophen-2-yl)malononitrile] (PFSDCN). The impact of the incorporation of monofunctional poly(ethylene glycol)-capped Au nanoparticles into the active layer of the polymer blend was specifically investigated. In the active layer of the polymer solar cell, the strong localized plasmonic resonance near field is distributed laterally along the active layer. Suitable optimization of the experimental conditions lead to an enhancement of the power conversion efficiency by 32%. Highly ordered honeycomb structures have also been fabricated with pre-synthesized nanoparticles by a patterning strategy based on formation of "breath figures". Oleic acid coordinated nanoparticles have been embedded in a polymeric matrix and the resulting nanocomposite solutions were fabricated in highly regular hexagonal microporous self-standing films. The fundamental role of the nanoparticle in stabilizing the water droplets during breath figure formation was confirmed. The plasmonic absorption of these films shows a broader band than that observed for the corresponding non-porous film., Such features can be accounted for by considering the convolution of two distinct contributions, the surface plasmon resonance peak of Au nanoparticles and the honeycomb structuring of the film. These highly ordered arrays have great potential as efficient catalysts for chemical reactions and as templates for the fabrication of photonic and optoelectronic devices, sensors, separation and purification membranes, and Raman spectroscopy substrates.[168]

5. Photo-thermal effects in metallic nanoparticles

Plasmonic nanoparticles have the extraordinary capability to convert external light to heat, as the strong electric field generated around the nanoparticles due to the localized plasmonic resonance effect is transformed, resulting in nanoscale sources of heat.[169] Since nanoparticles have a very low optical quantum yield (i.e. they are very poor light emitters), the total amount of heat generated can be estimated in a relatively simple manner by considering the total optical absorption. The photo-thermal properties of nanoparticles have historically been considered a side effect in plasmonic studies since these are typically focused on the optical properties. Scientists have only recently realized that this effect provides an unprecedented way to control thermal-induced phenomena at the nanoscale [170]. The heat generation process involves both the absorption of incident photons associated with the localized plasmonic resonance mechanism and the heat transfer from the nanoparticles to the surrounding matrix. Although challenging to measure the temperature increase at the surface of nanoparticles under optical illumination, it is an important issue for

applications ranging from nanomedicine to photonics. In this section, we first describe the physics of heat generation in plasmonic nanoparticles under optical illumination and then review recent attempts of exploiting (and measuring) this phenomenon for thermal-based therapies using optical excitation.

a Physics of plasmonic heating

If the wavelength (λ) of the incident light is much longer than the nanoparticle radius (R), the power absorbed (P) by a single nanoparticle can be expressed using the absorption cross-section σ_{abs} (see section 2):

$$P = \sigma_{abs}.I \tag{11}$$

where *I* is the irradiance of the impinging light. For simplicity, we consider the case of a spherical metal nanoparticle with a complex relative permittivity ε(ω) immersed in a dielectric medium with a real relative permittivity ε_m ($\varepsilon_m = n_m^2$; n_m is the refractive index of the surrounding medium). In case of a plane wave, $I = n_s c_0 \varepsilon_0 E_0^2/2$ where c_0 is the speed of light while E_0 is the amplitude of the external electric field.

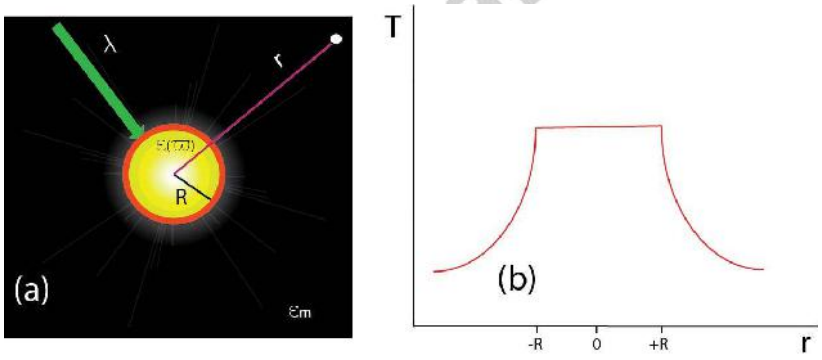

Figure 17: Schematic of the photo-thermal conversion process in a spherical nanoparticle (**a**) along with its temperature distribution (**b**).

The external radiation induces Joule heating on the nanoparticle yielding a heat power density *p(r)* given by:

$$p(r) = \frac{1}{2}\mathrm{Re}\left[J^*(r).E_{\mathrm{int}}(r)\right] \tag{12}$$

where J(r) is the complex amplitude of the electronic current density inside the nanoparticle while $E_{int}(r)$ is the inner electric field and r is the distance from the center of the sphere as shown in Figure 17. Using $J(r)=i\omega P$ and $P=\varepsilon_0\varepsilon(\omega)E$ results in::

$$p(r) = \frac{\omega}{2}\mathrm{Im}(\varepsilon(\omega))\varepsilon_0 \left|E_{\mathrm{int}}(r)\right|^2 \quad (13)$$

The electric field inside the nanoparticle can be easily expressed in terms of the external electric field through the expression:

$$E_{\mathrm{int}} = \frac{3\varepsilon(\omega)}{\varepsilon(\omega) + 2\varepsilon_m} E_0 \quad (14)$$

The heat generation is proportional to the square of the inner electric field of the nanoparticle. It is also important to point out that if the absorption cross section is known (e.g. nanoparticle with spherical geometry), P can be easily calculated by means of Equation (11). For more complicated geometries (e.g. rod-like nanoparticle), a numerical model for evaluating $E_{int}(r)$ is required in order to evaluate *p(r)* from Equation 13. The temperature profile under continuous wave illumination and in the absence of a phase transition can be described by means of the well-known heat transfer equation:

$$\nabla.\left[k(r)\nabla T(r)\right] = -p(r) \qquad r<R \quad (15)$$

$$\nabla.\left[k(r)\nabla T(r)\right] = 0 \qquad r>R \quad (16)$$

where *k (r)* and R are the thermal conductivity and the radius of the sphere respectively. It is easy to show (see reference 171 for details) that for a spherical nanoparticle, the temperature increase is given by:

$$\Delta T(r) \approx \Delta T_{NP} \qquad r<R \quad (17)$$

$$\Delta T(r) \approx \Delta T_{NP}\frac{R}{r} \qquad r>R \quad (18)$$

where ΔT_{NP} is the temperature increase of the nanoparticle. It is worth noting that although the heat power density *p(r)* can be non-uniform within the nanoparticle (according to equation 13), the temperature at equilibrium is uniform inside the nanoparticle (equation 15). This can be explained by taking into account the much higher thermal conductivity of metals with respect to the surrounding dielectric medium (water, polymer, etc…). It is easy to show (see reference [171] for details) that the temperature increase of a uniform charged sphere dispersed in a homogeneous medium with a thermal conductivity k_m is given by:

$$\Delta T_{NP} = \frac{P}{4\pi k_m R} \quad (19)$$

and consequently equation 18 can be written as:

$$\Delta T(r) \approx \frac{P}{4\pi k_m r} \tag{20}$$

The 1/r dependence of ΔT(r) outside the sphere leads to an infinite amount of thermal energy stored in the surrounding medium (Figure 17b). It is important to mention that for non-spherical nanoparticles, there is no simple analytical expression for the temperature increase and numerical simulations are critically fundamental to the discussion [171].

b Plasmonic photo-thermal therapy

Hyperthermia is a type of medical treatment in which body tissue is exposed to slightly higher temperatures (above 40°C) to damage and kill cancer cells. It has been exploited at a preclinical level in combination with radiation therapy. Light-induced hyperthermia exploits the lower thermal tolerance of cancer cells due to their reduced blood supply. Hyperthermic treatments using commercially available instruments are often limited to shallow penetration depths [172] (<3 cm), low treatment temperatures, and regions of the body with regular surface composition. Invasive approaches using microwave antennas are highly susceptible to interference, while magnetic particle treatments require large doses. Photothermal therapy, [173,174] however, is a minimally invasive treatment method in which photon energy is converted to thermal energy sufficient to induce cellular hyperthermia. Selectivity is achieved by focused directional control or invasive [175,176] (fiber optic) positioning of the incident light source The light source is either pulsed [177,178] or continuous wave laser radiation [177,179] and the treatment is typically accompanied by preferential administration of photoactive molecules [180,181] or nanoparticles. Photoexcitation of these results in non-radiative relaxation and local heat transfer to the surrounding tumor environment. In contrast, photodynamic therapy [182,183] relies on non-radiative relaxation through local formation of cytotoxic singlet oxygen species. While photothermal and photodynamic therapy treatments have garnered significant attention, such methods are inherently limited by photobleaching effects and weak absorption cross-sections. In the last ten years, nanoparticles have enabled a remarkable breakthrough in fighting cancer through the exploitation of the localized plasmonic resonance mechanism. Nanoparticles can be injected into the bloodstream and accumulate at tumor sites where they heat the local environment when irradiated with laser light whose wavelength coincides with the localized plasmonic resonance. Adjacent healthy tissue without embedded nanoparticles is unaffected by laser light alone. Cancer cells in the direct

vicinity of the nanoparticles undergo hyperthermia and death resulting in a new “drug-free” cancer therapy called plasmonic photothermal therapy.[184] In these cancer therapy applications, nanoparticles are useful due to their enhanced absorption cross-section (four to five orders of magnitude larger) as compared to conventional photoabsorbing dyes [185]. This strong absorption ensures effectiveness at lower radiation energy levels rendering the therapy method minimally invasive. In addition, nanoparticles have higher photostability and do not suffer from photobleaching.

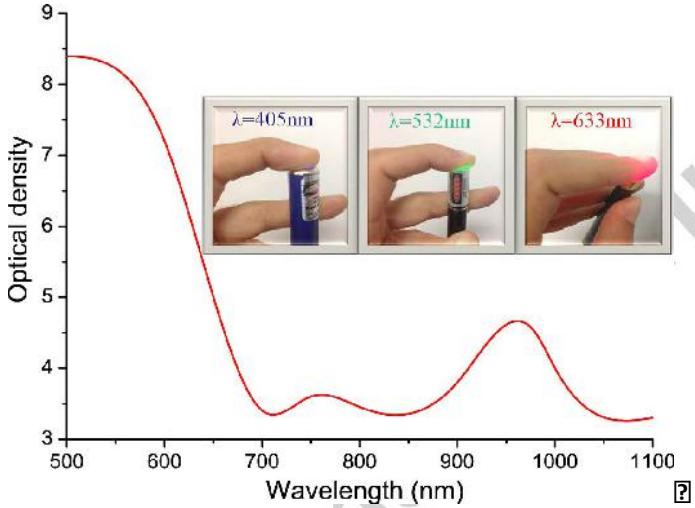

Figure 18: Absorption spectrum of a human hand along with the propagation of visible light in living tissue (inset).

In Figure 18, blue, green and red 5 mW lasers are placed on human fingers to visually examine how much light can be transmitted through roughly 1cm of finger tissue. The red laser light goes deep into the tissue while the green and blue laser light is absorbed by the tissue and consequently converted to heat energy. This visual observation is confirmed by examination of human hand absorption spectrum (Figure 18). When bridging biosystems and nanomaterials, it is important to keep the localized plasmonic resonance of the nanoparticles close to the first water transparency window (700-900 nm) where tissue absorption is low and penetration depth is high.[186] Au nanorods and nanoshell systems are particularly interesting since their localized plasmonic resonance can be tuned from the visible to near-infrared depending on their aspect ratio and size. Preparations have shown considerable efficacy for tumor ablation using near-infrared light, with the most recent data showing complete resorption of ~55% and ~25% of irradiated tumors, respectively.[187,188] Near-infrared plasmonic photothermal therapy using Au nanorods was first demonstrated by El-Sayed in 2006 through *in vitro* studies.[22] The Au nanorods were functionalized with anti-epidermal growth factor receptor (EGFR) antibodies for specific binding to EGFR-positive human oral cancer cells. After exposure to a beam of focused near-infrared light, the

cancer cells were destroyed without affecting the normal cells. The same group also demonstrated the feasibility of utilizing poly(ethylene glycol) capped Au nanorods for photothermal ablation of tunors using a human oral cancer xenograft mouse model.[188] In a different experiment, Park et al. [189] demonstrated the use of Au nanorods in plasmonic photothermal therapy experiments employingnude mice bearing bilateral human MDA-MB-435 tumors using either poly(ethylene glycol) - Au nanorods or a saline solution. The right flank of each mouse was irradiated for 5 min (810 nm, 2 W/cm^2) and all tumors were measured at regular intervals over time.

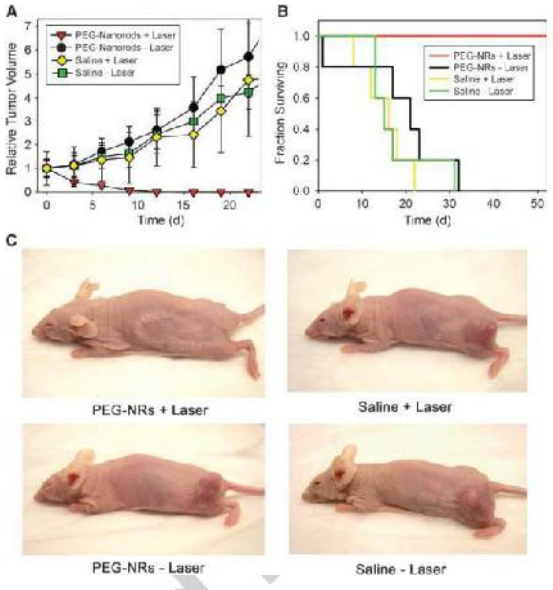

Figure 19: Photothermal destruction of human tumors in mice using long-circulating Au nanorods. **(A)** volumetric changes in tumor sizes are plotted over time after irradiation. **(B)** mice harboring one MDA-MB-435 human tumor were injected with either saline or poly(ethylene glycol) - Au nanorods and irradiated as in A. Survival of mice after irradiation is plotted versus time after irradiation. **(C)** at 20d after irradiation, near- infraredirradiated, all poly(ethylene glycol) - Au nanorods -injected mice showed only a minor scar and no evidence of tumor regrowth whereas all other treatment groups harbored thriving tumors. Reprinted with permission from ref. [189].

Within 10 days, all the irradiated, poly(ethylene glycol) - Au nanorod targeted tumors completely disappeared whereas all other tumors including those exposed to laser radiation after saline injection continued to grow uninhibited (Figure 19A). To assess the survival benefit of these capability, mice bearing a single MDA-MB-435 tumor were divided between four groups (poly(ethylene glycol) - Au nanorod + laser, poly(ethylene glycol) - Au nanorod - laser, saline + laser, saline - laser) and all tumors were measured over time (Figure 19B). After 20 days of treatment, all irradiated, poly(ethylene glycol) - Au nanorod injected mice displayed only a minor scar with no evidence of tumor regrowth, whereas all other surviving mice harbored thriving tumors (Figure 19B and C). Over the course of >50 days of observation, no irradiated (poly(ethylene glycol)- Au nanorod injected mice showed any evidence of recurrence whereas all mice in the

control groups were euthanized by day 33. The use of Au nanoshells was first developed by Hirsch et al. in 2003[190] in experiments working with subcutaneous U373 (human glioma cells) tumors.[191]

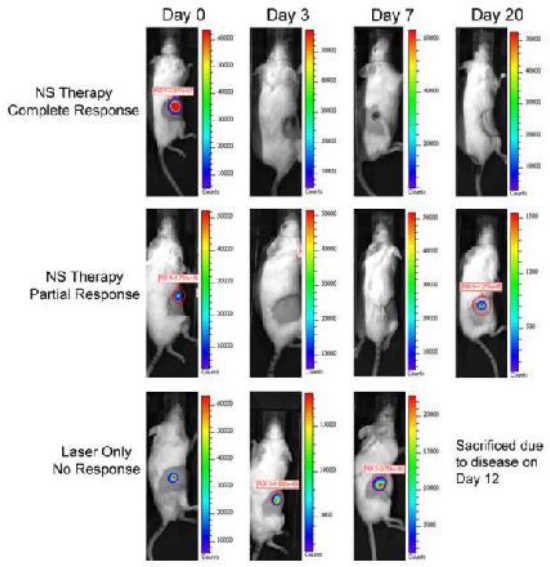

Figure 20: Bioluminescent imaging of tumors following laser irradiation. The mouse in the first row displayed loss of luminescence within 3 days of nanoshell therapy and remained tumor-free for the remainder of the study. The mouse in the second row experienced partial response to nanoshell therapy evidenced by initial loss in signal intensity but the tumor later recurred. The third row shows a mouse from the control group in which signal intensity and tumor burden increased following laser irradiation. Reprinted with permission from ref. [191].

Following laser irradiation, tumor growth and regression was measured daily using both bioluminescent imaging and caliper measurements to measure cellular development and changes in size. When the tumor reached 10 mm diameter, the mice were euthanized. Increased survival rates occurred for the Au nanoshell as indicated in Figure 20. The mouse shown in the first row of Figure 20 received Au nanoshell-assisted laser therapy and displayed complete tumor regression without any signs of regrowth for the entire period of study. The mouse in the second row also received Au nanoshell-mediated photothermal therapy and is an example of a partial responder, evidenced by initial loss in signal intensity during the first week following laser irradiation with subsequent reappearance of tumor cell luminescence by day 20 post-irradiation. The third row shows a mouse from the control group in which signal intensity and tumor burden increased following laser irradiation.

c. Nanoscale thermometers

A strong limitation to the application of nanoparticles for hypothermia is that for temperatures above 42°C, cell death also occurs in healthy tissues near the tumor site. The possibility of damage to healthy tissue is a serious risk and thus there is clear need to measure with

high sensitivity (less than 0.5°C) the local temperature of the illuminated area. Direct temperature measurement has been obtained by means of thermal camera analysis [192]. Despite its high sensitivity (≈ 0.2°C), the technique possesses limited spatial resolution (10-15µm) enabling only surface measurement of the temperature. Scanning thermal microscopy, using a modified atomic force microscope to map temperatures with 50 nm resolution requires tip contact with the sample to measure the temperature. Imaging techniques that do not require any direct contact with the sample have been recently developed based on optical methods including Raman spectroscopy, fluorescence intensity or fluorescence time correlation. None of these techniques combines the desired features of reliability, fast readout rate and high-resolution. In order to overcome such limitations, Baffou et al. [193] developed a new optical technique which delivers real-time, highly reliable, detailed images based on fluorescence polarization anisotropy. A fluorescent molecule absorbs light at a certain wavelength (e.g. green light) and after a short time delay, re-emits the light at a slightly longer wavelength (e.g. red). If the absorbed light is linearly polarized, the re-emitted light will be linearly polarized in the same direction. Since these molecules are immersed in a liquid, thermal fluctuations (Brownian motion) continuously change their position and consequently, the re-emitted light polarization is slightly different from the incident light polarization. At higher temperature, molecules move faster and thus the re-emitted light is more depolarized.

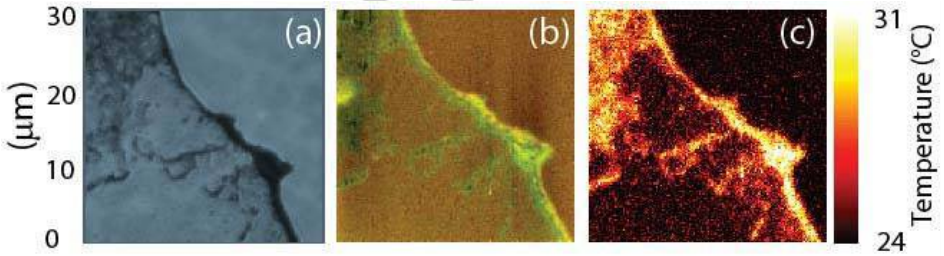

Figure 21: Optical image of dispersed and agglomerated nanorods (**a**). Fluorescence polarization anisotropy of the fluorescein molecules surrounding the Au nanorods (**b**) and sensing the temperature variations (**c**). Temperature map calculated from image (**b**). Reprinted with permission from ref. [193].

This technique was performed on an ensemble of colloidal Au nanorods to mimic the actual distribution obtained in cells. A drop of nanorod containing solution was deposited on a glass substrate and the residual solvent was allowed to evaporate slowly. The sample was covered with a glycerol-water-fluorescein solution and irradiated with polarized 770 nm laser radiation (chosen to match the longitudinal Au nanorods localized plasmonic resonance). Figure 21a shows an optical image recorded with a CCD camera at the edge of a drop. Figure 21b displays both fluorescence polarization maps overlapped using a color convention where green and red correspond to parallel

and orthogonal fluorescence polarizations, respectively. The associated temperature map is displayed in Figure 21c**.** No temperature variations are observed outside the drop edge (upper right part) which is as expected since no Au nanorods were present in this region. In a different approach, Okabe et al. [194] reported intracellular mapping of temperature by measuring the excited state lifetime of a water-sensitive methylacrylamide (DBD-AA) carried by a small (8–9 nm) fluorescent polymeric nanogel. The temperature resolution was ~ 0.4°C and calibration was performed in extracts of COS7 (fibroblast-like) cells. The results did not appear to depend on the probe concentration, proteins in the extracts, or the viscosity of the medium.

De Sio et. al. [148] recently demonstrated the possibility of monitoring nanoscale temperature variations under optical illumination by combining thermotropic cholesteric liquid crystals with Au nanorods. Cholesteric liquid crystals are an anisotropic fluid material that exhibits self-organizing properties which can respond to a wide variety of external perturbations (AC, DC, optical fields and pressure). A helical, macroscopic ordering of the molecules due to molecular chiral interactions between liquid crystal molecules leads to strong nascent coloration caused by structural interference. Small changes to this mesoscopic helical ordering results in stark differences in the local color of the film. Cetyltrimethylammonium bromide capped, water dispersible Au nanorods were synthesized and subsequently transferred in chloroform. 100μm thick glass cells were filled at room temperature by capillary action with a homogeneous solution of Au nanorods (10 wt.%) mixed with a cholesteric liquid crystals fluid (helix pitch of about 400 nm).

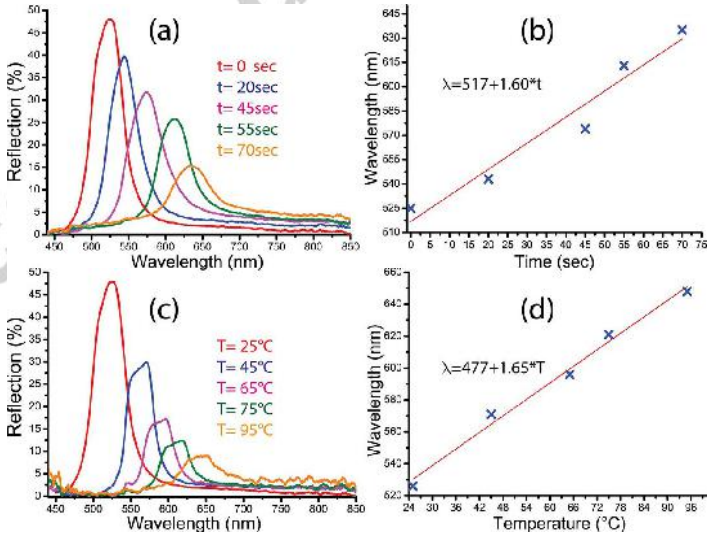

Figure 22: Reflection spectra of the sample for different values of illumination time (**a**) and temperature (**c**); linear fit of the position of the center of the reflection band versus illumination time (**b**) and temperature (**d**). Reprinted with permission from ref. [148]

The spectral reflection properties of the cholesteric liquid crystal configuration have been analyzed by probing with a white light source while irradiating the thin film with continuous wave near-infrared pump laser emitting at λ=680 nm (P_{pump}= 0.2 W/cm^2), chosen to because it resides in the high absorption range of the Au nanorods (longitudinal band). Figure **22a** reports the behavior of the reflection band under illumination with the pump beam, for different exposure times (from 0 sec up to 75 sec). The film acts as a mirror (the mesoscopic cholesteric liquid crystal helix axis oriented perpendicular to the glass surfaces) for all the wavelengths within the reflection band of the impinging white light (thus reflection intensity is high). Optically pumping the same sample area photoexcites the Au nanorods which induces conversion of light to heat (the mechanism is the same one described in section 5a) which is subsequently transferred to the cholesteric liquid crystal fluid. Figure 22a shows that keeping the pump power constant and increasing the exposure time results in a gradual increase of the local temperature as indicated by a linear red shift (more than 130 nm, Figure 22b) of the reflection peak wavelength and partial suppression of the reflection band intensity. This is confirmed in a control experiment where the sample temperature was raised from 25°C to 95°C (Figure **22c**) and a clear linear red-shift in peak wavelength was observed. It is worth noting that the two calibration functions reported in Figure 22b and 22d exhibit, the same linear behavior indicating it is possible to measure the temperature around Au nanorods with a sensitivity of about 0.03 °C.

6. Nanoscale optoelectronic circuits

The rapid miniaturization of electronics to the submicron scale has led to tremendous increases in computing power while at the same time enabling cost reduction. As the microelectronic industry advances toward ever smaller devices, it is reasonable to believe that both physical and economic factors of top-down silicon technology will soon limit further advances. To go beyond these limits and fuel the expected demands of future society will require revolutionary breakthroughs rather than continued, current evolutionary progress. One of the most promising solutions is replacing electronic signals with light. However, a major problem with using electromagnetic waves as information carriers in optical signal-processing devices and integrated circuits is the low level of integration and miniaturization available. This problem is connected to the diffraction limit of light in dielectric media, which does not allow for the confinement of electromagnetic waves into nanoscale regions much smaller than the wavelength of light. One fascinating way to localize the optical radiation into a nanometer-sized volume is by using the unique properties of plasmonic nanomaterials. They are an effective bridge between bulk materials and atomic/molecular structures

as indicated by their very intense colors , notably absent from both similar bulk and individual atoms. The physics behind this behavior can be explained by considering the collective oscillation of the free conduction electrons induced by an interacting external electromagnetic field (localized plasmonic resonance as introduced in section 2). The plasmonic coupling between metallic nanoparticles and light enables a universal range of interesting optical phenomena such as plasmonic circuits [195], biosensing [196] and quantum information processing. [197] In this section, we overview recent advances in modern electronic circuits based on plasmonic properties such as nanoantennas, perfect plasmonic absorbers and integrated nanocircuits.

a. Nano-antennas

An antenna is a device used to propagate, receive, and/or transmit electromagnetic waves which can have information embedded within them□They are important elements of wireless information transmission networks along with the sources and detectors of the electromagnetic waves. Optical nanoantennas are the visible spectrum counterpart of microwave and radio frequency antennas. The term nano-antenna has been coined in the modern literature. A receiving nano-antenna is a device effectively converting incident light (optical frequency radiation) into a strongly confined field. Conversely, a transmitting antenna converts a strongly confined field in the optical frequency range of a source (weakly emitting or almost non-emitting) into optical radiation.

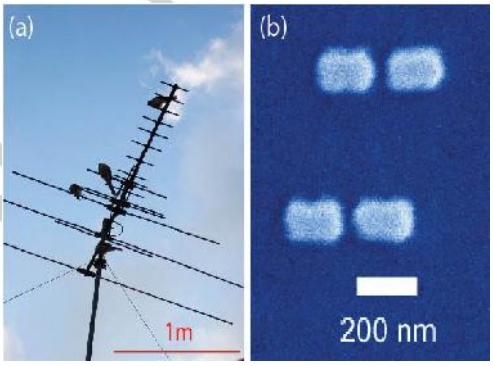

Figure 23: Examples of an radio frequency (**a**) and optical (**b**) antenna. (**b** is credit to O Muskens).

Figure 23 shows a comparison between a radio frequency antenna and an optical nano-antenna. Radio frequency antennas with features on the order of several centimeters are important devices in modern communication. Optical nano-antennas, with feature sizes on the order of a few hundred nanometers, find several important applications due to strong electric field (localized plasmonic resonance effect) localized at the nanoscale. In 1985, Wessel [198] showed that a metallic nanoparticle can behave as an antenna. He suggested that a single plasmonic particle may

allow the diffraction limit of optical devices to be overcome and predicted future resolving powers down to 1 nm. In the current literature [199], such nano-antennas are usually referred to as monopoles (Figure **24**), especially in the discussion of the interaction between the antenna and a quantum object.

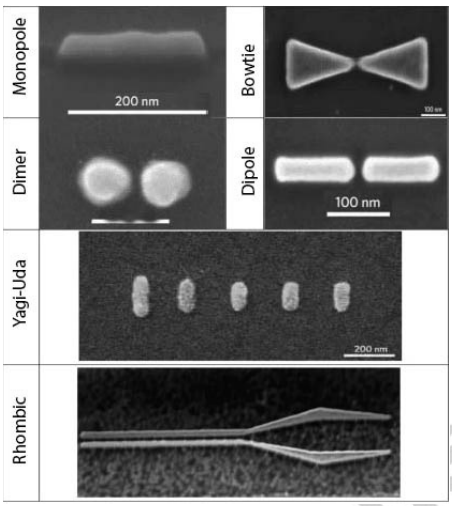

Figure 24: Different types of plasmonic nano-antennas. Reprinted with permission from ref. [199].

The magnitude of the near field in the gap between two or more plasmonic nanoparticles can be an order of magnitude higher than in the vicinity of an elongated nanoparticle. The enhancement of the electric field in the gap strongly depends on the metal, the geometry of the nanoparticles, the gap width, the radius of the curvature of the nanoparticle surface within the gap, and the local dielectric properties of the environment. A large variety of systems of differing geometries and operational principles have been explored. Dimer nano-antennas that consist of two nanoparticles (Figure 24) are of particular interest. This large class includes dipole nano-antennas and `Bowtie' nano-antennas, so named for the similarity in appearance to the well-known garment. One problem facing nanophotonics frequently requires that a given emitter radiate only in a desired direction. This requirement is met using Yagi-Uda nano-antennas (Figure 24), part of a general class of rhombic nano-antennas (Figure 24) [200] which are analogous to rhombic RF antennas. Figure 25 shows a plasmonic waveguide which gradually widens in size towards one end and thus leads to directional emission. The authors also report results of numerical simulations of a wireless communication system utilizing two rhombic nano-antennas shown in the schematic arrangement on a glass substrate presented in Figure 25b. Results of the numerical simulations shown in Figure 25c indicate a major part of the power radiated by the antenna also enters the substrate.

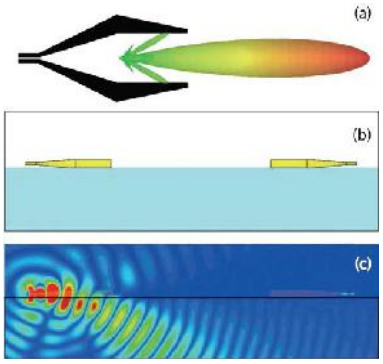

Figure 25: Rhombic nano-antenna: (**a**) design and directivity diagram; (**b**) arrangement of two nano-antennas on a glass substrate, and (**c**) results of numerical simulation of a wireless system for data transfer between two rhombic nano-antennas. Reprinted with permission from ref. [200].

b. Plasmonic absorbers

Plasmonic metamaterials have drawn the attention of the scientific community in the last decade for a number of applications including negative refractive index [201], cloaking devices [202] and data storage [203]. Complete absorption of light, realized by designing a medium whose impedance matches that of free space while being opaque, is a recent addition to the property space being examined. If such a medium is filled with a lossy medium, the resulting structure can absorb light totally in a sharp or broad frequency range. There have been increased theoretical and experimental efforts that serve to show how nanoparticle arrays or metamaterial resonators and periodic structures are useful in boosting the overall absorption in both solar panels and semiconductor substrates.[204] Most of these structures are inherently sensitive to the frequency of operation and they are typically narrowband as they are based on the introduction of highly resonant electric and magnetic elements on top of lossy dielectric and metallic substrates.[205] Efficient coupling of both the electric and magnetic fields inside the substrate leads to enhanced absorption at a resonance frequency. Remarkable effort has been devoted toward the realization of broadband absorption operation by utilizing tapered metallic geometries or by combining multiple resonances.[206] All of the currently proposed solutions still exhibit bandwidth limitations since they are fundamentally based on resonant mechanisms.

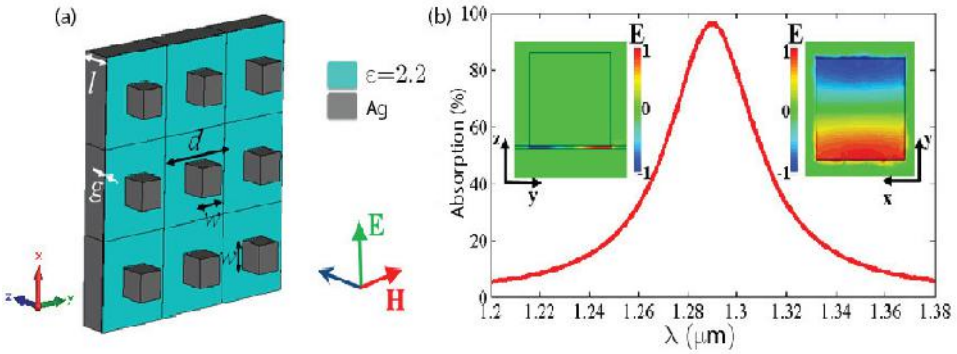

Figure 26: Film-coupled plasmonic nano-antenna array with a dielectric material loaded at the spacer layer (**a**). Percentage of absorption versus the wavelength of the impinging radiation. The normalized electric field distributions at the resonant absorption peak are shown in two cross-sections in the inset. Standing waves are formed inside the gap between the metallic cube and the silver film (**b**). Reprinted with permission from ref. [207].

Recently, Argyropoulos [207] proposed an example of a narrowband absorber realized in a two-dimensional (2D) metamaterial (Figure 26). It was composed of well-organized metallic Ag cubes separated from a silver film with a dielectric spacer layer. The fields are perfectly coupled and confined inside the nanogaps created between the cubes and the film at the resonance frequency. Coupling of the magnetic and electric fields results in the destructive interference of the reflected waves and subsequently, very little radiation is reflected from the surface. Due to the presence of the silver film, the structure is opaque to propagating external radiation (the transmission coefficient is almost zero). Consequently, 'perfect' absorption is obtained at the resonance frequency of this plasmonic device. The geometry of this film-coupled plasmonic nanocube absorber is shown in Figure 26a and has dimensions of w = 80nm, d = 250nm, g = 2nm and l = 100nm. The cube and the metallic film are made of silver with dielectric properties as reported in the reference.[208] A dielectric surrounding material is included as the spacer layer with a relative permittivity of ε= 2.2. The plasmonic structure is simulated with commercial software (CST) based on a finite-integration method. The absorption, plotted in Figure 26b, has a pronounced peak of almost perfect absorption obtained at the resonant wavelength of about λ=1.3μm. The quality factor of this resonance is approximately Q≈60, a typical value for plasmonic resonators. Two cross-sections of the normalized field distributions are depicted in the inset of Figure 26b at the resonant wavelength. It is clear that a first-order Fabry-Perot mode is formed between the nanocube and the metallic film which leads to trapped fields inside the nanocavities and enhanced absorption at this particular frequency point.

An exciting way to improve the performance of existing infrared and optical absorbers is based on an array of plasmonic nano-antennas. This approach has a number of potential

applications such as thermal emitters, sensors, spatial light modulators and optical communication elements. Self-assembled nano-antenna arrays separated from a metallic film by a thin insulating layer can offer strong localization of electromagnetic radiation and may lead to new types of efficient light-trapping structures used in conjunction with thin-film solar cell devices.[209] A significant amount of research recently has been focused on developing plasmonic absorbers with extended working frequency (broadband) where the performance is dictated by the engineering design. It is very hard to reconfigure the device or tune the absorption bands without redesigning the structure and repeating the fabrication process.

Active control (i.e. dynamic modulation) of the localized plasmonic resonance of nanoparticles is a crucial step toward the realization of nanodevices for manipulating light at the nanoscale. In particular, dynamically modulating the dielectric properties of the surrounding medium has attracted interest due to large scale versatility. Liquid crystals have been examined in this context as their local refractive index can be easily modified by using electrical and thermal stimuli. Several examples of voltage control of the localized plasmonic resonance properties have been reported in the last few years where either the nanoparticles have been dissolved in the liquid crystal fluid [210] or have been immobilized onto a substrate, which then utilizes an 'active' liquid crystal overlayer.[211] All the methods to date do not provide a strong change since the localized plasmonic resonance oscillation is confined onto a 30-40 nm thick layer at the surface and the LC director reorientation near the surface can be rather small compared to the bulk due to strong anchoring at the functionalized surfaces. De Sio et al. [212] demonstrated an efficient way to overcome these drawbacks through the use of a photo-alignment layer, whose local orientation can be modulated by using suitable polarized light. The few nanometer thick film acts as a command layer for controlling the liquid crystal order directly on the surface, thus localizing a variation in the liquid crystal refractive index around the Au nanorods.

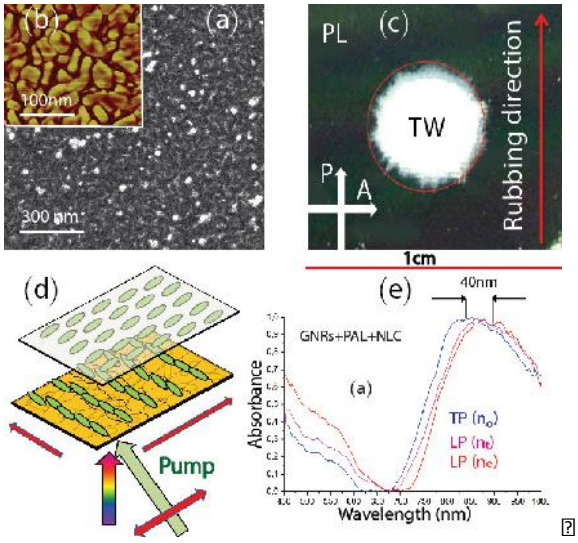

Figure 27: Scanning electron microscope view (**a**) and atomic microscope view topography (**b**) of the Au nanorodsdistribution before the photo-alignment layer deposition; polarized optical microscope view of the planar (**c,** outside the red circle) and twist (**c,** inside the red circle) of the sample between crossed polarizers. Sketch of the nematic liquid crystal alignment in twisted configuration (**d**) along with its spectral response (**e**) after the external pump irradiation. Reprinted with permission from ref. [212]

An external light source was used for controlling the localized plasmonic resonance of a large scale Au nanorod array, immobilized on a glass substrate, which was covered in a second step by a thin layer of photo-alignment material. This surface was then used as one of the substrates in the fabrication of an aligned nematic liquid crystal cell. Modulation of the local alignment of the photo-alignment layer using polarized light was shown to modify the local nematic liquid crystal refractive index which subsequently led to a shift of the transverse plasmonic resonance of the system. Figure 27a, a scanning electron microscope image of the Au nanorod distribution before the photo-alignment layer deposition shows a well dispersed and almost equally spaced rods of ~ 2.9 ± 0.4 aspect ratio. The Au nanorods appear randomly distributed and exhibit no discernible organization on the surface as deposited. The polydispersity of the Au nanorod monolayer distribution was evaluated by means of statistical analysis of the particle population using atomic force microscopy phase images, an example which is shown in Figure 27b. The Au nanorod substrate was then covered with a photo-alignment layer and a nematic liquid crystal film was sandwiched between the treated Au nanorod substrate and a top glass surface coated with a conventional thin rubbed polyimide layer. Figure 27b is a polarized optical microscope view of the sample where the original, planarly aligned area is outside the circled region. The white circle corresponds to an area which has been exposed for 30 s to a polarized continuous wave laser (λ=488, P= 0,3 W/cm^2) which reorients the photo-alignment layer, affecting the local liquid crystal orientation. When photo-aligning molecules are optically pumped by a polarized light beam parallel

to their absorption oscillators, they become excited and relax multiple times, eventually leading to the reorientation of the photo-alignment layer molecules (perpendicular to the polarization of the impinging light) orthogonal to the initial alignment (see the sketch in Figure 27d). The same area of the liquid crystal cell shown in Figure 27c has been illuminated with a pump light (λ=488, P= 0,3 W/cm^2, t=200s) in order to induce a planar to twist nematic liquid crystal reorientation. The refractive index of the twisted configuration is the average between the nematic liquid crystal ordinary and extraordinary values ($n_t \approx 1.6$) and is thus different in the reoriented state. Consequently, the longitudinal plasmon band is different (Figure magenta curve) and resides between the ones obtained for the two starting polarizations (Figure 27e, blue curve), (Figure 27e, red curve) before the illumination.

c. Nano-optical integrated circuits

New discoveries in materials on the nanometer length scale are expected to play a very important role in addressing ongoing and future research in the field of modern electronics. Unprecedented data bandwidth, ever falling power consumption requirements, and reduced cost margins of on-chip photonics have established a photonic roadmap for scaling down photonic components. A solution to fulfill both size and power requirements for future photonic integrated circuit technologies lies in photonic components scaled beyond the diffraction limit of light. In order to address these requirements, photonic components and even electronic circuits based on localized plasmonic resonance have been proposed and are showing promise for the scalability and performance challenges of future photonic integrated circuits (Figure 28).

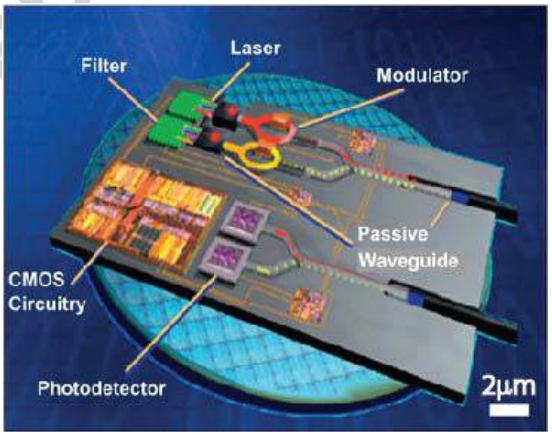

Figure 28: Schematic of plasmonic integrated circuit components featuring high functionality on small wafer footprints. Reprinted with permission from ref. [195].

A huge variety of plasmonic waveguides have been proposed and investigated for the general purpose of on-chip communication.[195] Nanoscale metallic particle chains offer subwavelength fields by operating at the surface plasmon frequency, yet suffer from optical losses yielding very short propagation distance.[213] Different research groups, motivated by the strong lateral confinement observed in metal nanowires [214], have investigated surface plasmon propagation along metal waveguides with 2D nanostructures. plasmon lasers are a potential solution to the challenge of finding suitable surface plasmon sources for ultra-compact plasmonic circuits.[215] Surface plasmon lasers operate by amplification of surface plasmons instead of light, and, consequently, show distinct operation features compared to classical lasers. The confined electromagnetic fields within a plasmonic laser cavity allow for extremely compact devices which have been shown to dramatically enhance the spontaneous emission rate due to the Purcell effect, which quantifies the enhancement of the spontaneous emission rate of an emitter relative to its free-space value.[216] On a plasmonic photonic integrated circuit, data packages have to be converted from the optical to the electrical domain by a photodetector. For photonic-plasmonic hybrid circuits, there are a number of important reasons why such an integrated plasmonic detector provides advantages over conventional detectors. The plasmonic detector can be of nanoscale dimensions, offering multiple advantages including higher integration densities, low device capacitance for fast transit times, higher bandwidth operation, and reduced energy to operate. In this framework, Yi et al. [217] very recently demonstrated that the localized optical energy in nanoplasmonic resonators can be efficiently converted to mechanical energy and actuate nanomechanical structures for infrared thermal detector applications. A schematic of the plasmomechanical device with optical readout is shown in Figure 29.

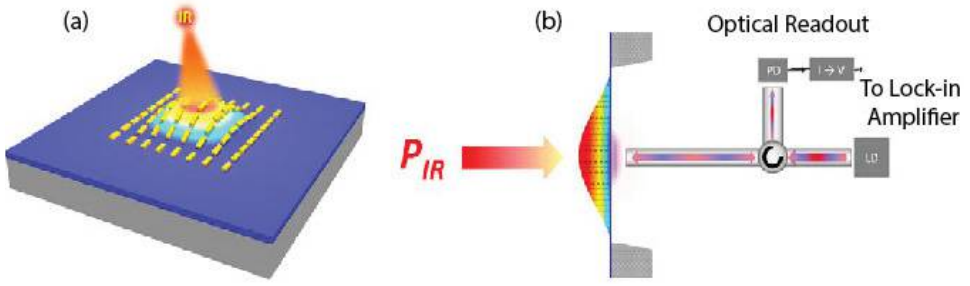

Figure 29: A schematic overview of the membrane based plasmomechanical infrared detector: (**a**) a plasmonic antenna absorber is formed by fabricating Au nanorod antennas on a commercial silicon nitride membrane. (**b**) The membrane also acts as one of the two reflectors of a fiber optic interferometer. The optical readout is formed by a 1550 nm laser (LD), a photodetector (PD), a current to voltage converter (I→V) and a lock-in amplifier. The infrared power, PIR, is supplied by a 6 μm laser. Reprinted with permission from ref. [217]

An Au nanorod antenna absorber fabricated on a silicon nitride membrane, a well-known mechanical resonator platform [218], forms the central part of the device. The resonant wavelength of the plasmonic antenna absorber is tuned to 6 μm. On resonance, the plasmonic antenna absorber efficiently converts incoming infrared radiation into thermal energy. Due to the mismatch between the thermal expansion coefficients of the silicon nitride membrane and the Au nanorods, the increased temperature caused by this infrared absorption drives the membrane to mechanically deflect. This deflection can be read out optically by a fiber-optic interferometer based on a Fabry–Perot cavity formed by the backside of the membrane and the end face of a bare fiber.[219] The total reflectivity of the interferometer is highly sensitive to the distance between the two reflectors. Light from a 1550 nm laser is coupled into the interferometer through a fiber-optic circulator and the reflected optical power is converted into signal current by a photodetector.

7. Conclusions

Plasmonic materials represent a potential building block component for the next generation of photonic and optoelectronic devices. They provide a plethora of physical phenomena which are important for various areas of optical physics and photonic technologies and have the potential to play a unique and important role in enhancing the processing speed of future integrated circuits. Tremendous synergy can be attained by integrating plasmonic, electronic, and conventional dielectric photonic devices on the same chip and taking advantage of the strengths of each. To this end, we have reviewed recent results obtained in the field of plasmonic technologies based on nanomaterials. We assert that the unique optical properties and capabilities of plasmonic nanomaterials have been successfully applied to a number of application areas in the last few years. The coupling of plasmonic nanostructure design, the composition of the plasmonic material, and appropriate synthesis and fabrication techniques has fostered the experimental realization of a variety of functional structures. We have shown the temperature increase of nanoparticles under suitable optical illumination has application in local temperature monitoring and thermal-based medical therapies. We also reported on recent advances in modern electronic circuits exploiting plasmonic properties including nano-antennas, perfect plasmonic absorbers and integrated nanocircuits. Further work has the promise to efficiently exploit solar energy and lighting, to increase data capacity and the speed of optical communication systems, and eventually lead to dynamically reconfigurable photonic and optoelectronic components.

8. Acknowledgments

We acknowledge the cooperation of all co-authors of the papers we published on the argument: R. Bartolino, C. Umeton (from the University of Calabria) and co-workers; T. Bürgi (from the Université de Genève) and co-workers; A. Agostiano (from University of Bari-Chemistry Department) and co-workers. The research was supported by the Air Force Office of Scientific Research (AFOSR), Air Force Research Laboratory (AFRL), U.S. Air Force, under grant FA9550-14-1-0050 (P.I. L. De Sio, EOARD 2014/2015) and the Materials and Manufacturing Directorate, AFRL; the Sens&Micro LAB Project (POFESR 2007-2013), PRIN 2010-2011 (Prot. 2010C4R8M8) and PRIN 2012 (Prot. 2012T9XHH7).

9. References

[1] A. Moores, F. Goettmann New J. Chem. 30 (2006) 1121-1132.

[2] U. Kreibig, M. Vollmer, Optical Properties of Metal Clusters, , Springer (1995), Berlin.

[3] C. F. Bohren, D. R. Huffman: Absorption and Scattering of Light by Small Particles, Wiley (1983), New York.

[4] C.-K. Sun, F. Vallée, L.H. Acioli, E.P. Ippen, J.G. Fujimoto, Phys.Rev. B 50 (1994) 15337–15348.

[5] L.M. Liz-Marzan, Mater. Today 7 (2004) 26-31.

[6] K.L. Kelly, E. Coronado, L.L. Zhao, G.C. Schatz, J. Phys. Chem. B 107 (2003) 668-677.

[7] U. Kreibig, L. Genzel, Surf. Sci. 156 (1985) 678-700.

[8] E. Hutter, J.H. Fendler, Adv. Mater. 16 (2004) 1685-1706.

[9] G. Mie, Ann. Phys. (Leipzig) 25 (1908) 377-445.

[10] J.W.S. Rayleigh:Phil. Mag. 41 (1871) 274-279.

[11] P. Drude Annalen der Physik. 1 (1900) 566.

[12] A. Sommerfeld, Annalen der Physik (4th series) 28 (1909) 44.

[13] C. Noguez, J. Phys. Chem. C 111 (2007) 3806-3819.

[14] G.A. López-Muñoz, J.A. Pescador-Rojas, J. Ortega-Lopez, J. Santoyo Salazar, J.A. Balderas-López, Nanoscale Res. Lett.7 (2012) 423.

[15] R. Gans, Ann. Phys. (Leipzig) 352 (1915) 270-281.

[16] K.H. Su, Q.H. Wei, X. Zhang, J.J. Mock, D.R. Smith, S. Schultz, Nano Lett. 3 (2003) 1087-1090.

[17] W. Rechberger, A. Hohenau, A. Leitner, J.R. Krenn, B. Lamprecht, F.R. Aussenegg, Opt. Commun. 220 (2003) 137-141.

[18] M.A. El-Sayed, Acc. Chem. Res. 34 (2001) 257-264.

[19] S. Link, M.A. El-Sayed, Annu. Rev. Phys. Chem. 54 (2003) 331-366.

[20] C.J. Murphy, T.K. Sau, A.M. Gole, C.J. Orendorff, J. Gao, L. Gou, S.E. Hunyadi, T. Li, J. Phys. Chem. B 109 (2005) 13857-13870.

[21] S. Link, M.A. El-Sayed, J. Phys. Chem. B 103 (1999) 8410-8426.

[22] X. Huang, I.H. El-Sayed, W. Qian, M.A. El-Sayed, J. Am. Chem. Soc. 128 (2006) 2115-2120.

[23] M. Tréguer-Delapierre, J. Majimel, S. Mornet, E. Duguet, S. Ravaine, Gold Bull. 41 (2008) 195-207.

[24] J. Neddersen, G. Chumanov, and T. Cotton, Appl. Spectrosc. 47 (1993) 1959-1964.

[25] V. Amendola and M. Meneghetti, Phys. Chem. Chem. Phys. 11 (2009) 3805–3821.

[26] S. Besner, A.V. Kabashin, F.M. Winnik and M. Meunier, J. Phys. Chem. C 113 (2009) 9526-9531.

[27] J.B. Herzog, M.W. Knight, and D. Natelson, Nano Lett. 14 (2014) 499−503.

[28] M.P. Jonsson and C. Dekker, Nano Lett. 13 (2013) 1029−1033.

[29] M. Okumura, S. Tsubota, M. Iwamoto and M. Haruta, Chemistry Letters (1998) 315-316.

[30] V. Resta, A.P. Caricato, A. Loiudice, A. Rizzo, G. Gigli, A. Taurino, M. Catalano, M. Martino, J Nanopart Res 15 (2013) 2017.

[31] C.L. Haynes, R.P. van Duyne, J. Phys. Chem. B 105 (2001) 5599-5611.

[32] S.M. Yang, S.G. Jang, D.G. Choi, S. Kin, H.K. Yu, Small 2 (2006) 458-475.

[33] B.J.Y. Tan, C.H. Sow, T.S. Koh, K.C. Chin, A.T.S. Wee, C.K. Ong, J. Phys. Chem. B 109 (2005) 11100-11109.

[34] S. Rusponi, G. Costantini, F. Buatier-de-Mongeot, C. Boragno, U. Valbusa, Appl. Phys. Lett. 75 (1999) 3318- 3320.

[35] B. Fazio, C. D'Andrea, F. Bonaccorso, A. Irrera, G. Calogero, C. Vasi, P. G. Gucciardi, M. Allegrini, A. Toma, D. Chiappe, C. Martella, and F. Buatier de Mongeot, AcsNano 5 (2011) 5945–5956.

[36] H. Zhang, C.A. Mirkin, Chem. Mater. 16 (2004) 1480-1484.

[37] L. Qin, S. Park, L. Huang, C.A. Mirkin, Science 309 (2005) 113-115.

[38] S.I. Bozhevolnyi, V.S. Volkov, E. Devaux, J.Y. Laluet, T.W. Ebbesen, Nature 440 (2006) 508-511.

[39] C. Murphy, A.M. Gole, S. Hunyadi, C. Orendorff, Inorg. Chem. 45 (2006) 7544-7554.

[40] C. Burda, X. Chen, R. Narayan, M.A. El-Sayed, Chem. Rev. 105 (2005) 1025-1102.

[41] Y. Sun, Y. Xia, Science 298 (2002) 2176-2179.

[42] S.E. Skrabalak, J. Chen, L. Au, X. Lu, X. Li, Y. Xia, Adv. Mater. 19 (2007) 3177-3184.

[43] S. Oldenburg, R.D. Averitt, S.L. Westcott, N.J. Halas, Chem. Phys. Lett. 288 (1998) 243-247.

[44] S. Shankar, S. Bhargav, M. Sastry, J. Nanosci. Nanotech. 5 (2005) 1721-1727.

[45] E. Hao, R.C. Bailey, G.C. Schatz, J. Hupp, S. Li, NanoLett. 4 (2004) 327-330.

[46] L.A. Austin, M.A. Mackey, E.C. Dreaden, M.A. El‑Sayed, Arch. Toxicol. 88 (2014) 1391–1417.

[47] M.C. Daniel, D. Astruc, Chem. Rev. 104 (2004) 293-346.

[48] J. Turkevich, P. Stevenson, J. Hillier, Discuss. Faraday Soc. 11 (1951) 55-75.

[49] M. Brust, M. Walker, D. Bethell, D.J. Schiffrin, R. Whyman, J. Chem. Soc. Chem. Commun. 7 (1994) 801–802.

[50] Y. Fang, J. Chem. Phys. 108 (1998) 4315–4318.

[51] A. Pyatenko, M. Yamaguchi, M. Suzuki, J. Phys. Chem. C 111 (2007) 7910–7917.

[52] E. Braun, Y. Eichen, U. Sivan and G. Ben-Yoseph, Nature 391 (1998) 775-778.

[53] J. Sloan, D.M. Wright, H.G. Woo, S. Bailey, G. Brown, A.P.E. York, K.S. Coleman, J.L. Hutchison and M.L.H. Green, Chem. Commun. (1999) 699.

[54] M.H. Huang, A. Choudrey and P. Yang, Chem. Commun. (2000) 1063.

[55] S. Bhattacharrya, S.K. Saha and D. Chakravorty, Appl. Phys. Lett. 76 (2000) 3896-3898.

[56] V.M. Cepak and C.R. Martin, J. Phys. Chem. B 102 (1998) 9985-9990.

[57] J.C. Hulteen, C.R. Martin, J. Mater. Chem. 7 (1997) 1075-1087.

[58] P. Zhao, N. Li, D. Astruc, Coordination Chemistry Reviews 257 (2013) 638–665.

[59] J. Pérez-Juste, I. Pastoriza-Santos, L.M. Liz-Marzán, P. Mulvaney, Coord. Chem. Rev. 249 (2005) 1870-1901.

[60] Y.Y. Yu, S.-S. Chang, C.-L. Lee, C.R.C. Wang, J. Phys. Chem. B 101 (1997) 6661-6664.

[61] N.R. Jana, L. Gearheart, C.J. Murphy, J. Phys. Chem. B 105 (2001) 4065-4067.

[62] B. Nikoobakht, M.A. El-Sayed, Chem. Mater. 15 (2003) 1957-1962.

[63] N.R. Jana, Small 1 (2005) 875-882.

[64] F. Kim, J.H. Song, P. Yang, J. Am. Chem. Soc. 124 (2002) 14316-14317.

[65] T. Placido, R. Comparelli, F. Giannici, P.D. Cozzoli, G. Capitani, M. Striccoli, A. Agostiano and M.L. Curri, Chem Mater 21 (2009) 4192–4202.

[66] Y.-J. Zhu, X.-L Hu, Chem. Lett. 32 (2003) 1140-1141.

[67] B.D. Busbee, S.O. Obare, C.J. Murphy, Adv. Mater. 15 (2003) 414-416.

[68] C.J. Johnson, E. Dujardin, S.A. Davis, C.J. Murphy, S. Mann, J. Mater. Chem. 12 (2002) 1765-1770.

[69] C.J. Murphy, T.K. Sau, A. Gole, C.J. Orendorff, MRS Bull. 30 (2005) 349-355.

[70] J. Gao, C.M. Bender, C.J. Murphy, Langmuir 19 (2003) 9065-9070.

[71] J.E. Millstone, W. Ei, M.R. Jones, H. Yoo, C.A. Mirkin, Nano Lett. 8 (2008) 2526–2529.

[72] C.J. Johnson, E. Dujardin, S.A. Davis, C.J. Murphy, S. Mann, J. Mater. Chem. 12 (2002) 1765–1770.

[73] J. Pèrez-Juste, L.M. Liz-Marzan, S. Carnie, D.Y.C. Chan, P. Mulvaney, Adv. Funct. Mater. 14 (2004) 571–579.

[74] S. Si, C. Leduc, M.H. Delville, B. Lounis, ChemPhysChem 13 (2012) 193–202.

[75] M.Z. Liu, P. Guyot-Sionnest, J. Phys. Chem. B 109 (2005) 22192-22200.

[76] F. Giannici, T. Placido, M.L. Curri, M. Striccoli, A. Agostiano, R. Comparelli, Dalton Trans. (2009) 10367-10374.

[77] E. Carbò-Argibay, B. Rodriguez-Gonzalez, S. Gomez-Grana, A. Guerrero-Martinez, I. Pastoriza-Santos, J. Perez-Juste, L.M. Liz-Marzan, Angew. Chem. Int. Ed. 49 (2010) 9397–9400.

[78] M.A. Mahmoud, M.A. El-Sayed, J. Gao, U. Landman, Nano Lett. 13 (2013) 4739–4745.

[79] J. Zhang, M.R. Langille, M.L. Personick, K. Zhang, S. Li, C.A. Mirkin, J. Am. Chem. Soc. 132 (2010) 14012–14014.

[80] J. Chen, D. Wang, J. Xi, L. Au, A. Siekkinen, A. Warsen, Z.-Y. Li, H. Zhang, Y. Xia, X. Li, Nano Lett. 7 (2007) 1318–1322.

[81] Y. Sun, Y. Xia, Science 298 (2002) 2176–2179.

[82] M.P. Melancon, W. Lu, Z. Yang, R. Zhang, Z. Cheng, A.M. Elliot, J. Stafford, T. Olson, J.Z. Zhang, C. Li, Mol. Cancer Ther. 7 (2008) 1730–1739.

[83] B. Van de Broek, N. Devoogdt, A. D'Hollander, H.-L. Gijs, K. Jans, L. Lagae, S. Muyldermans, G. Maes, G. Borghs, ACS Nano 5 (2011), 4319–4328

[84] D. Y. Kim, T. Yu, E. C. Cho, Y. Ma, O. O. Park, Y. Xia, Angew. Chem. Int. Ed. 50 (2011) 6328 – 6331.

[85] L. Lu, K. Ai, Y. Ozaki, Langmuir 24 (2008) 1058 – 1063.

[86] N. Li, P. Zhao, and D. Astruc, Angew. Chem. Int. Ed. 53 (2014) 2–36.

[87] A.M. Gobin, M.H. Lee, N.J. Halas, W.D. James, R.A. Drezek, and J.L. West, Nano Lett. 7 (2007) 1929–1934.

[88] P.K. Jain, I.H. El-Sayed, and M.A. El-Sayed, Nanotoday 2 (2007) 18–29.

[89] G. Baffou, R. Quidant, and C. Girard, Applied Physics Letters 94 (2009) 153109.

[90] S.E. Lohse, N.D. Burrows, L. Scarabelli, L.M. Liz-Marzan, C.J. Murphy, Chem. Mater. 25 (2013) 1250-1261.

[91] R. Bardhan, W. Chen, C. Perez-Torres, M. Bartels, R.M. Huschka, L.L. Zhao, E. Morosan, R.G. Pautler, A. Joshi, N.J. Halas, Adv. Funct. Mater. 19 (2009) 3901–3909.

[92] T. Pham, B. Jackson, N.J. Halas, T.R. Lee, Langmuir 18 (2002) 4915–4920.

[93] C. Ayala-Orozco, J.G. Liu, M.W. Knight, Y. Wang, J.K. Day, P. Nordlander, and N.J. Halas, Nano Lett. 14 (2014) 2926-2933.

[94] S. Hong, J.A.I. Jr. Acapulco, H.Y. Jang, and S. Park, Chem. Mater. 26 (2014) 3618−3623.

[95] H. Li, X. Ma, J. Dong, W. Qian Anal. Chem. 81 (2009) 8916–8922.

[96] J. Zhou, L. Meng, Q. Lu J. Mater. Chem. 20 (2010) 5493–5498.

[97] W.Y. Li, P.H.C. Camargo, X.M. Lu, Y.N. Xia, Nano Lett. 9 (2009) 485–490.

[98] S. Kim, J. Jin, Y.-J. Kim, I.-Y. Park, Y. Kim, S.-W. Kim, Nature 453 (2008) 757–760.

[99] K. Ueno, S.;Juodkazis, V. Mizeikis, K. Sasaki, H. Misawa, Adv. Mater. 20 (2008) 26–30.

[100] K. Hirano, H. Shimizu, T. Enami, M. Terakawa, M. Obara, N.N. Nedyalkov and P.A. Atanasov, Journal of Nanotechnology in Diagnosis and Treatment 1 (2013) 2-10

[101] P. Muhlschlegel, H.-J. Eisler, O.J.F. Martin, B. Hecht, D.W. Pohl, Science 308 (2005) 1607–1609.

[102] E. Ozbay, Science 311 (2006) 189–193.

[103] N.L. Rosi, C.A. Mirkin, Chem. Rev. 105 (2005) 1547–1562.

[104] L. Shao, K. Choi Woo, H. Chen, Z. Jin, J. Wang, and H.-Q. Lin ACSNano 2010, 4, 3053–3062.

[105] L. Gunnarsson, T. Rindzevicius, J. Prikulis, B. Kasemo, M. Kall, S. Zou, G.C. Schatz, J. Phys. Chem. B 109 (2005) 1079-1087.

[106] P.K. Jain, W. Huang, M.A El-Sayed, Nano Lett. 7 (2007) 2080-2088.

[107] C.J. Loweth, W.B Caldwell, X. Peng, A.P. Alivisatos, P.G. Schultz, Angew. Chem., Int. Ed. 38 (1999) 1808-1812.

[108] J.P. Novak, D.L. Feldheim, J. Am. Chem. Soc. 122 (2000) 3979-3980.

[109] B. Li, C.Y. Li, J. Am. Chem. Soc. 129 (2007) 12-13.

[110] X. Xu, N.L.Rosi, Y. Wang, F. Huo, C.A. Mirkin, J. Am. Chem. Soc. 128 (2006) 9286-9287.

[111] R. Sardar, T.B. Heap, J.S. Shumaker-Parry, J. Am. Chem. Soc. 129 (2007) 5356-5357.

[112] J.P. Spatz, S. Moessmer, M. Moeller, Chem. Eur. J. 2 (1996) 1552-1555.

[113] A. Baron, A. Iazzolino, K. Ehrhardt, J.-B. Salmon, A. Aradian, V. Kravets, A.N. Grigorenko, J. Leng, A. Le Beulze, M. Tréguer-Delapierre, M.A Correa-Duarte, P. Barois, Opt. Mater. Express 3 (2013) 1792-1797.

[114] E. Fanizza, N. Depalo, L. Clary, A. Agostiano, M. Striccoli, M.L. Curri, Nanoscale 5 (2013) 3272-3282.

[115] R.I. Nooney, D. Thirunavukkarasu, Y. Chen, R. Josephs, A.E. Ostafin, Langmuir 19 (2003) 7628-7637.

[116] C. Ingrosso, A. Panniello, R. Comparelli, M.L. Curri, M. Striccoli, Materials 3 (2010) 1316-1352.

[117] R. Comparelli, M.L. Curri, P.D. Cozzoli, M. Striccoli, in: C.S.S.R. Kumar (Ed.), Nanomaterials for Biosensors Vol. 8 Nanotechnologies for the Life Sciences, WILEY-VCH, Weinheim (2006) 123-174.

[118] C.M. McIntosh, E.A. Esposito, A.K. Boal, J.M. Simard, C.T. Martin, V.M. Rotello, J. Am. Chem. Soc. 123 (2001) 7626–7629.

[119] X.H. Huang, P.K. Jain, I.H. El-Sayed, M.A. El-Sayed, Photochem. Photobiol. 82 (2006) 412–417.

[120] Y. Yuan, J. Zhang, H. Zhang, X. Yang, Analyst 137 (2012) 496–501.

[121] C.K. Kim, P. Ghosh, C. Pagliuca, Z.-J. Zhu, S. Menichetti, V.M. Rotello, J. Am. Chem. Soc. 131 (2009) 1360–1361.

[122] L.H. Dubois, R.G. Nuzzo, Annu. Rev. Phys. Chem. 43 (1992) 437–463.

[123] K.E. Sapsford, W.R. Algar, L. Berti, K.B Gemmill, B.J. Casey, E. Oh, M.H. Stewart, I.L. Medintz, Chem Rev 113 (2013) 1904–2074.

[124] Z. Amoozgar, Y. Yeo, Wiley Interdiscip. Rev. Nanomed. Nanobiotechnol. 4 (2012) 219–233.

[125] J. Wang, J.D. Byrne, M.E. Napier, J.M. De Simone, Small 7 (2011) 1919–1931.

[126] A.P. Alivisatos, K.P. Johnsson, X.G. Peng, T.E.,Wilson, C.J. Loweth, M.P. Jr. Bruchez, P.G. Schultz, Nature 382 (1996) 609–611.

[127] N.L. Rosi, D.A. Giljohann, C.S. Thaxton, A.K.R. Lytton-Jean, M.S. Han, C.A. Mirkin, Science 312 (2006) 1027–1030.

[128] L.A. Austin, B. Kang, C.-W. Yen, M.A. El-Sayed, Bioconjugate Chem. 22 (2011) 2324–2331.

[129] Z. Liu, F. Kiessling, J. Gatjens, J. Nanomater. (2010) doi:10.1155/2010/894303).

[130] X.M. Qian, X.H. Peng, D.O. Ansari, Q. Yin-Goen, G.Z. Chen, D.M. Shin, L. Yang, A.N. Young, M.D. Wang, S. Nie, Nat. Biotechnol. 26(2008) 83–90.

[131] M. Fischler, A. Sologubenko, J. Mayer, G. Clever, G. Burley, J. Gierlich, T. Carell and U. Simon (2008) Chem Commun 2:169–171.

[132] J.R. Dunklin, G.T. Forcherio, K.R.Jr. Berry, and D.K. Roper, J. Phys. Chem. C 118 (2014) 7523–7531.

[133] V. Reboud, G. Leveque, M. Striccoli, T. Placido, A. Panniello, M.L. Curri, J.A. Alducin, T. Kehoe, N. Kehagias, D. Mecerreyes, S.B. Newcomb, D. Iacopino, G. Redmond, C.M.S. Torres, Nanoscale 5 (2013) 239-245.

[134] M.L. Curri, R. Comparelli, M. Striccoli, A. Agostiano, Phys. Chem. Chem. Phys. 12 (2010) 11197-11207.

[135] W.W. Weare, S.M. Reed, M.G. Warner, and J.E. Hutchison, J. Am. Chem. Soc. 122 (2000) 12890-12891.

[136] A. Kumar, S. Mandal, P.R. Selvakannan, R. Pasricha, A.B. Mandale, and M. Sastry, Langmuir 19 (2003) 6277-6282.

[137] M. Brust, N. Stuhr-Hansen, K. Nørgaard, J.B. Christensen, L.K. Nielsen, and T. Bjørnholm Nano Lett. 1 (2001) 189-191.

[138] H. Yao, O. Momozawa, T. Hamatani, and K. Kimura, Chem. Mater. 13 (2001) 4692-4697.

[139] M.K. Corbierre, N.S. Cameron, M. Sutton, K. Laaziri, and R. B. Lennox, Langmuir 21 (2005) 6063-6072.

[140] S. Pierrat, I. Zins, A. Breivogel, and C. Sönnichsen, Nano Lett. 7 (2007) 259-263.

[141] T. Placido, R. Comparelli, M. Striccoli, A. Agostiano, A. Merkoci, M.L. Curri, Sensors Journal, IEEE 13 (2013) 2834-2841.

[142] T. Placido, G. Aragay, J. Pons, R. Comparelli, M.L. Curri, A. Merkoçi, ACS Appl. Mater. Interfaces 5 (2013) 1084-1092.

[143] C. Yu, J.Irudayaraj, Anal. Chem. 79 (2006) 572-579.

[144] T. Teranishi, I. Kiyokawa, M. Miyake, Adv. Mater. 10 (1998) 596-599.

[145] M. Sastry, A. Kumar, P. Mukherjee, Colloids and Surfaces A: Physicochem. Eng. Aspects 181 (2001) 255–259.

[146] M. Jebb, P.K. Sudeep, P. Pramod, K.G. Thomas, and P.V. Kamat, J. Phys. Chem. B 111 (2007) 6839-6844.

[147] J. Yang, J. Wu, Y. Wu, J. Wang, C. Chen, Chem. Phys. Lett. 416 (2005). 215-219.

[148] L. De Sio, T. Placido, S. Serak, R. Comparelli, M. Tamborra, N. Tabiryan, M.L. Curri, R. Bartolino, C. Umeton, and T. Bunning, Adv. Optical. Mater. 1 (2013) 899-904.

[149] V. Reboud, N. Kehagias, M. Striccoli, T. Placido , A.M. Panniello, M.L. Curri, M. Zelsmann, F. Reuther, G. Gruetzner and C.M. Sotomayor Torres, Journal of Vacuum Science & Technology B 25 (2007) 2642-2644.

[150] A. Sanchot, G. Baffou, R. Marty, A. Arbouet, R. Quidant, C. Girard, E. Dujardin, ACS Nano 6 (2012) 3434–3440.

[151] H Wang, X. Song, C. Liu, J. He, W.H. Chong, H. Chen 8 (2014) 8063–8073.

[152] K.M. Schulz, S. Abb, R. Fernandes, M. Abb, A.G. Kanaras, O.L. Muskens, Langmuir 28 (2012) 8874–8880.

[153] A. Klinkova, R.M. Choueiri, E. Kumacheva, Chem. Soc. Rev. 43 (2014) 3976-3991.

[154] A.F. Stewart, A. Lee, A. Ahmed, S. Ip, E. Kumacheva, G.C. Walker, ACS Nano 24 (2014) 5462- 5467.

[155] P. D. Cozzoli, E. Fanizza, M. L. Curri, D. Laub, A. Agostiano Chem. Commun. (2005) 942–944.

[156] M. Corricelli, N. Depalo, E. Fanizza, D. Altamura, C. Giannini, D. Siliqi, R. Di Mundo, F. Palumbo, V. Kravets, A. Grigorenko, A. Agostiano, M. Striccoli, M. L. Curri, J. Phys. Chem. C. 18 (2014) 7579-7590.

[157] R.A. Alvarez-Puebla, A. Agarwal, P. Manna, B.P. Khanal, P. Aldeanueva-Potel, E. Carbó-Argibay, N. Pazos-Pérez, L. Vigderman, E.R. Zubarev, N.A. Kotov, L. M. Liz-Marzán PNAS 108 (2011) 8157-8161.

[158] J. Xiao, Z. Li, X. Ye, Y. Ma, L. Qi, Nanoscale 6 (2014) 996–1004.

[159] S. Gómez-Graña, J. Pérez-Juste, R.A. Alvarez-Puebla, A. Guerrero-Martínez, L.M. Liz-Marzán, Adv. Optical Mater. 1 (2013) 477–481.

[160] L. Malassis, P. Massé, M. Tréguer-Delapierre, S. Mornet, P. Weisbecker, V. Kravets, A. Grigorenko, P Barois, Langmuir 29 (2013) 1551–1561.

[161] T. Jägeler-Hoheisel, J. Cordeiro, O. Lecarme, A. Cuche, C. Girard, E. Dujardin, D. Peyrade, A. Arbouet, J. Phys. Chem. C 117 (2013) 23126−23132.

[162] T. Placido, E. Fanizza, P. Cosma, M. Striccoli, M.L. Curri, R. Comparelli, A. Agostiano, Langmuir 30 (2014) 2608-2618.

[163] A. Kuzyk, R. Schreiber, Z. Fan, G. Pardatscher, E.M. Roller, A. Högele, F.C. Simmel, A.O. Govorov, T. Liedl, Nature 483 (2012) 311–314.

[164] M. Li, S.K. Cushing, J. Zhang, S. Suri, R. Evans, W.P. Petros, L.F. Gibson, D. Ma, Y. Liu, N. Wu, ACS Nano 7 (2013) 4967–4976.

[165] S.Z. Nergiz, S. Singamaneni, ACS Appl. Mater. Interfaces 3 (2011) 945-951.

[166] S. Bhattacharyya, S. Prashanthi , P. R. Bangal , A. Patra J. Phys. Chem. C 117 (2013) 26750-26759.

[167] S.W. Tong, C.F. Zhang, C.Y. Jiang, G. Liu, Q.D. Ling, E.T. Kang, D.S.H. Chan, C. Zhu, Chemical Physics Letters 453 (2008) 73-76.

[168] N. Depalo, M. Tamborra, E. Fanizza, D. Di Gioia, A. Agostiano, M.L. Curri, M. Striccoli, Science of Advanced Materials 6 (2014) 505-512.

[169] X. Huang, S. Neretina, M.A. El-Sayed, Adv. Mater. 21 (2009) 4880-4910.

[170] A.O. Govorov and H.H. Richardson, Nano Today 2 (2007) 30-38.

[171] G. Baffou, R. Quidant, and F.J. Garcıa de Abajo, ACS Nano 4, (2010) 709-716.

[172] P. Wust, B. Hildebrandt, G. Sreenivasa, B. Rau, J. Gellermann, H. Riess, R. Felix, P.M. Schlag, Lancet Oncol. 3 (2002) 487-597.

[173] A.L. Mckenziei, J.A.S. Carruth, Phys. Med. Biol. 29 (1984) 619-641.

[174] L.O. Svaasand, C.J. Gomer, E.A. Morinelli, Lasers Med. Sci. 5(1990) 121-128.

[175] Z. Amin, J.J. Donald, A. Masters, R. Kant, A.C. Steger, S.G. Bown, W.R. Lees, Radiology, 187 (1993) 339-347.

[176] K. Eichler, M.G. Mack, R. Straub, K. Engelmann, S. Zangos, D. Woitaschek, T.J. Vogl, Radiology 41 (2001) 915-922.

[177] C.M. Pitsillides, E.K. Joe, X. Wei, R.R. Anderson, C.P. Lin, Biophys. J. 84 (2003) 4023-4032.

[178] L. Tong, Y. Zhao, T.B. Huff, M.N. Hansen, A. Wei, J.X. Cheng, Adv. Mater. 19 (2007) 3136–3141.

[179] X. Huang, I.H. El-Sayed, M.A. El-Sayed, J. Am. Chem. Soc. 128 (2006) 2115-2120.

[180] W.R. Chen, R.L. Adams, K.E. Bartels, R.E. Nordquist, Cancer Lett. 94 (1995) 125-131.

[181] W.R. Chen, R.L. Adams, R. Carubelli, R.E. Nordquist, Cancer Lett. 115 (1997) 25-30.

[182] D. Dolmans, D. Fukumura, R.K. Jain, Nat. Rev. Cancer 3 (2003) 380-387.

[183] T.J. Dougherty, C.J. Gomer, B.W. Henderson, G. Jori, D. Kessel, M. Korbelik, J. Moan, Q. Peng, J. Nat. Cancer Inst. 90 (1998) 889-905.

[184] X. Huang, P.K. Jain, I.H. El-Sayed, M.A. El-Sayed, Nanomedicine 2 (2007) 681-693.

[185] W.R. Chen, R.L. Adams, E. Heaton, D.T. Dickey, K.E. Bartels, R.E. Nordquist, Cancer Lett. 88 (1995) 15-19.

[186] C.R. Simpson, M. Kohl, M. Essenpreis, M. Copey, Physics in Medicine and Biology 43 (1998) 2465-2468.

[187] W.D. James, L.R. Hirsch, J.L. West, P.D. O'Neal, J.D. Payne, J. Radioanal. Nucl. Ch. 271 (2007) 455-464.

[188] E.B. Dickerson, E.C. Dreaden, X. Huang, I.H. El-Sayed, H. Chu, S. Pushpanketh, J.F. McDonald, and M.A. El-Sayed, Cancer Lett. 269 (2008) 57-66.

[189] J.H. Park, G. von Maltzahn, L.L. Ong, A. Centrone, T.A. Hatton, E. Ruoslahti, S.N. Bhatia, and M.J. Sailor, Cancer Res. 69 (2009) 3892-3900.

[190] L.R. Hirsch, R.J. Stafford, J.A. Bankson, S.R. Sershen, R.E. Price, J.D. Hazle, N.J. Halas and J.L. West, Proc. Natl. Acad. Sci. USA 100 (2003) 13549-54.

[191] E.S. Day, P.A. Thompson, L. Zhang, N.A. Lewinski, N. Ahmed, R.A. Drezek, S.M. Blaney, J.L. West, Journal of Neuro. Oncology 104 (2011) 55-63.

[192] G. Baffou, P. Bon, J. Savatier, J. Polleux, M. Zhu, M. Merlin, H. Rigneault and S. Monneret, ACS Nano 6 (2012) 2452-2458.

[193] G. Baffou, M.P. Kreuzer, F. Kulzer, and R. Quidant, Optics Express 17 (2009) 3291-3298.

[194] K. Okabe, N. Inada, C. Gota, Y. Harada, T. Funatsu, S. Uchiyama, Nature Communications 3 (2012) 705.

[195] V.J. Sorger, R.F. Oulton, R.M. Ma and X. Zhang, MRS Bulletin, 37 (2012) 728-73.

[196] J.N. Anker, W.P. Hall, O. Lyandres, N.C. Shah, J. Zhao and R.P. Van Duyne, Nature Materials 7 (2008) 442 – 453.

[197] M.S. Tame, K.R. McEnery, Ş.K. Özdemir, J. Lee, S.A. Maier and M.S. Kim, Nature Physics 9 (2013) 329-340.

[198] J.J. Wessel, Opt. Soc. Am. B 2 (1985) 1538-1541.

[199] P. Biagioni, J.S. Huang and B. Hecht, Rep. Prog. Phys. 75 (2012) 024402-024478.

[200] M. Klemm, Int. J. Opt. 2012 (2012) 348306-348313.

[201] J.B. Pendry, Phys. Rev. Lett. 85 (2000) 3966-3969.

[202] J.B. Pendry, D. Schurig and D.R. Smith, Science 312 (2006) 1780-1782.

[203] M. Wuttig and N. Yamada, Nat. Mater. 6 (2007) 824-832.

[204] H.A. Atwater and A. Polman, Nat. Mater. 9 (2010) 205-213.

[205] N.I. Landy, S. Sajuyigbe, J.J. Mock, D.R. Smith, and W.J. Padilla, Phys. Rev. Lett. 100 (2008) 207402-207404.

[206] K. Aydin, V.E. Ferry, R.M. Briggs, H.A. Atwater, Nat. Commun., 2 (2011) 517-523.

[207] C. Argyropoulos, Forum for Electromagnetic Research Methods and Application Technologies (FERMAT) (2012) 1-14.

[208] P.B. Johnson, and R.W. Christy, Phys. Rev. B, 6 (1972) 4370-4379.

[209] S. Mokkapati, F.J. Beck, R. de Waele, A. Polman, and K.R. Catchpole, J. Phys. D Appl. Phys. 44 (2011) 185101-185109.

[210] L. De Sio, R Caputo, U. Cataldi, C. Umeton, J. Mater. Chem. 21 (2011) 18967-18970.

[211] L. De Sio, A. Cunningham, V. Verrina, C.M. Tone, R. Caputo, T. Burgi, C. Umeton, Nanoscale 4 (2012) 7619-7623.

[212] L. De Sio, G. Klein , S. Serak, N. Tabiryan, A. Cunningham, C.M. Tone, F. Ciuchi, T. Bürgi, C. Umeton, T. Bunning, J. Mater. Chem. C 1 (2013) 7483-7487.

[213] S.A. Maier , P.G. Kik, H.A. Atwater, S. Meltzer, E. Harel, Nat. Mater. 2 (2002) 229-232.

[214] F. Kusunoki, T. Yotsuya, J. Takahara, Opt. Express 14 (2006) 5651-5656.

[215] V.J. Sorger, X. Zhang, Science 333 (2011) 709-710.

[216] D. Genov, R. Oulton, G. Bartal, X. Zhang, Phys. Rev. B 83 (2011) 245312-245315.

[217] F. Yi, H. Zhu, J.C. Reed, A.Y. Zhu, and E. Cubukcu, IEE photonics technology letters 26 (2014) 202-205.

[218] P.L. Yu, T.P. Purdy, and C.A. Regal, Phys. Rev. Lett. 108 (2012) 0836031–0836035.

[219] O. Kilic, M. Digonnet, G. Kino, and O. Solgaard, Meas. Sci. Technol. 18 (2007) 3049-3054.